LOAD FREQUENCY CONTROL OF MULTIPLE-AREA POWER SYSTEMS

YAO ZHANG

Bachelor of Electrical Engineering

Tsinghua University

July, 2007

submitted in partial fulfillment of requirements for the degree

MASTER OF SCIENCE IN ELECTRICAL ENGINEERING

at the

CLEVELAND STATE UNIVERSITY

August, 2009

This thesis has been approved
for the Department of Electrical and Computer Engineering
and the College of Graduate Studies by

_____

Thesis Committee Chairperson, Dr. Lili Dong

_____

Department/Date

_____

Committee Member, Dr. Daniel Simon

_____

Department/Date

_____

Committee Member, Dr. Zhiqiang Gao

_____

Department/Date

_____

Committee Member, Dr. F. Eugenio Villaseca

_____

Department/Date

To
my beloved parents Xu Zhang and Ming Yao
and
my fiancée Yi Xu

ACKNOWLEDGEMENTS

LOAD FREQUENCY CONTROL OF MULTIPLE-AREA POWER SYSTEMS

YAO ZHANG

ABSTRACT

In an interconnected power system, as a power load demand varies randomly, both area frequency and tie-line power interchange also vary. The objectives of load frequency control (LFC) are to minimize the transient deviations in theses variables (area frequency and tie-line power interchange) and to ensure their steady state errors to be zeros. When dealing with the LFC problem of power systems, unexpected external disturbances, parameter uncertainties and the model uncertainties of the power system pose big challenges for controller design. Active disturbance rejection control (ADRC), as an increasingly popular practical control technique, has the advantages of requiring little information from the plant model and being robust against disturbances and uncertainties. This thesis presents a solution to the LFC problem based on ADRC. The controller is constructed for a three-area power system with different turbine units including non-reheat, reheat and hydraulic units in different areas. The dynamic model of the power system and the controller design based on the model are elaborated in the thesis. Simulation results and frequency-domain analyses proved that ADRC controller is attractive to the LFC problem in its stability and robustness.

TABLE OF CONTENTS

LIST OF TABLES

Table	Page

LIST OF FIGURES

Figure   **Page**

NOMENCLATURE

AC: Alternating current

ACE: Area control error

ADRC: Active disturbance rejection control

ESO: Extended state observer

GA: Genetic algorithm

GALMI: Genetic algorithm and linear matrix inequalities

GenCo: Generating company

LFC: Load frequency control

MEMS: Micro electromechanical system

PI: Proportional-integral

PID: Proportional-integral-derivative

TF: Transfer function

CHAPTER I

INTRODUCTION

1.1 Load frequency control

Power systems are used to convert natural energy into electric power. They transport electricity to factories and houses to satisfy all kinds of power needs. To optimize the performance of electrical equipment, it is important to ensure the quality of the electric power. It is well known that three-phase alternating current (AC) is generally used to transport the electricity. During the transportation, both the active power balance and the reactive power balance must be maintained between generating and utilizing the AC power. Those two balances correspond to two equilibrium points: frequency and voltage. When either of the two balances is broken and reset at a new level, the equilibrium points will float. A good quality of the electric power system requires both the frequency and voltage to remain at standard values during operation. For North America, the standard values for the frequency and voltage are *60 Hertz* and *120 Volts* respectively. However, the users of the

electric power change the loads randomly and momentarily. It will be impossible to maintain the balances of both the active and reactive powers without control. As a result of the imbalance, the frequency and voltage levels will be varying with the change of the loads. Thus a control system is essential to cancel the effects of the random load changes and to keep the frequency and voltage at the standard values.

Although the active power and reactive power have combined effects on the frequency and voltage, the control problem of the frequency and voltage can be decoupled. The frequency is highly dependent on the active power while the voltage is highly dependent on the reactive power. Thus the control issue in power systems can be decoupled into two independent problems. One is about the active power and frequency control while the other is about the reactive power and voltage control. The active power and frequency control is referred to as load frequency control (LFC) [1].

The foremost task of LFC is to keep the frequency constant against the randomly varying active power loads, which are also referred to as unknown external disturbance. Another task of the LFC is to regulate the tie-line power exchange error. A typical large-scale power system is composed of several areas of generating units. In order to enhance the fault tolerance of the entire power system, these generating units are connected via tie-lines. The usage of tie-line power imports a new error into the control problem, i.e., tie-line power exchange error. When a sudden active power load change occurs to an area, the area will obtain energy via tie-lines from other areas. But eventually, the area that is subject to the load change should balance it without external support. Otherwise there would be economic

conflicts between the areas. Hence each area requires a separate load frequency controller to regulate the tie-line power exchange error so that all the areas in an interconnected power system can set their setpoints differently. Another problem is that the interconnection of the power systems results in huge increases in both the order of the system and the number of the tuning controller parameters. As a result, when modeling such complex high-order power systems, the model and parameter approximations can not be avoided [2]. Therefore, the requirement of the LFC is to be robust against the uncertainties of the system model and the variations of system parameters in reality.

In summary, the LFC has two major assignments, which are to maintain the standard value of frequency and to keep the tie-line power exchange under schedule in the presences of any load changes [1]. In addition, the LFC has to be robust against unknown external disturbances and system model and parameter uncertainties. The high-order interconnected power system could also increase the complexity of the controller design of the LFC.

1.2 Existing load frequency control solutions

In industry, proportional-integral (PI) controllers have been broadly used for decades as the load frequency controllers. A PI controller design on a three-area interconnected power plant is presented in [3], where the controller parameters of the PI controller are tuned using trial-and-error approach.

The LFC design based on an entire power system model is considered as centralized method. In [4] and [5], this centralized method is introduced with a simplified multiple-area power plant in order to implement such optimization techniques on the entire model. However, the simplification is based on the assumption that all the subsystems of the entire power system are identical while they are not. The assumption makes the simulation model in the paper quite different from the real system. Another problem for the centralized methods is that even if the method works well on a low-order test system, it would face an exponentially increasing computation problem with the increase of the system size.

Since the tie-line interfaces give rise to weakly coupled terms between areas, the large-scale power system can be decentralized into small subsystems through treating tie-line signals as disturbances. Numerous control techniques have been applied to the decentralized power systems. In [6–10], decentralized PI or proportional-integral-derivative (PID) controller is reported. Since H_2/H_∞ control is well known for its robustness against parameter uncertainties, the controller has been utilized to solve the decentralized LFC problems in [11–14]. There are also several other modern control theories that have been decentralized solutions of the LFC problem, such as disturbance accommodation control, optimal tracking approach, predictive control scheme and ramp following control, which can be found in [15–18] respectively.

Fuzzy logic control is a method based on fuzzy set theory, in which the fuzzy logic variables can be any value between 0 and 1 instead of just true and false. When the variables are selected, the decision will be made through specific fuzzy logic functions. Research

results obtained from applying the fuzzy logic control technique to the decentralized LFC problem have been proposed in [19–22]. Specifically, a fuzzy logic controller developed directly from a fuzzy model of the power system is reported in [19]. A fuzzy logic based tie-line bias control scheme on a two-area multiple-unit power system is introduced in [20] while a similar method on a combined cycle power plant including the comparison between the fuzzy logic control and conventional PID control techniques are reported in [21]. A fuzzy-gain-scheduled PI controller and its implementation on an Iraqi National Super Grid power system can be found in [22]. A comparison between the fuzzy-gain-scheduled PI controller and the traditional PI controller was also included in [22].

Genetic algorithm (GA) is one of the most popular computer intelligence algorithms. It has been verified to be effective to solve complex optimization problem [23] where PI-type controllers tuned via GA and linear matrix inequalities (GALMI) is presented on a decentralized three-area nine-unit power system. In [23], it is found that the structure of the GALMI tuned PI controller is much simpler than that of the H_2/H_∞ controller although the performances of the two methods are equivalent.

Most of the reported solutions of the LFC problem have been tested for their robustness against large step load change. However, very few of the published researches deal with parameter uncertainties. In [2], the authors set up a 15% floating rate for the parameters in one area and successfully controlled the system with an optimally tuned PID controller. Nevertheless, in [2], a lot of approximations and simplifications have been made during the modeling process of the power systems, on which the controller is designed. The

simplified system model has deviated far from the real system. A control technique with a notable robustness against not only parameter uncertainties but also model uncertainties and external load change will be preferred by the power industry.

1.3 Active disturbance rejection control

Active disturbance rejection control (ADRC), an increasingly popular practical control technique, was first proposed by J. Han in [24] and has been modified by Z. Gao in [25, 26]. The design of ADRC only relies on the most direct characteristics of a physical plant, which are input and output. Specifically, the information required for the control purpose is analyzed and extracted from the input and output of the system. ADRC generalizes the discrepancy between the mathematical model and the real system as a disturbance, and rejects the disturbance actively, hence the name active disturbance rejection control. Since ADRC is independent of the precise model information of the physical system, it is very robust against parameter uncertainties and external disturbances [27].

As discussed in [25], ADRC can be understood as a combination of an extended state observer (ESO) and a state feedback controller, where the ESO is utilized to observe the generalized disturbance, which is also taken as an augmented/extended state, and the state feedback controller is used to regulate the tracking error between the real output and a reference signal for the physical plant. In addition, a concept of bandwidth parameterization is proposed in [25] to minimize the number of tuning parameters of ADRC. Using this concept, ADRC only has two tuning parameters, of which one is for the controller, and the

other is for the observer. The two tuning parameters directly reflect the response speeds of the ESO and the closed-loop control system respectively. The few tuning parameters also make the implementation of ADRC feasible in practice. The detailed explanations about how to select the tuning parameters for ADRC are provided in [26].

At the beginning of the research of ADRC, time-domain analyses of the controller dominated the publications about it. Recently, a transfer function representation of ADRC was initially presented in [27], where frequency-domain analyses have been successfully conducted on a second-order linear plant. In [27], an equivalent block diagram of ADRC controlled closed-loop system was developed, as shown in Figure 1. The definitions of the transfer function blocks in Figure 1 can be found in [27].
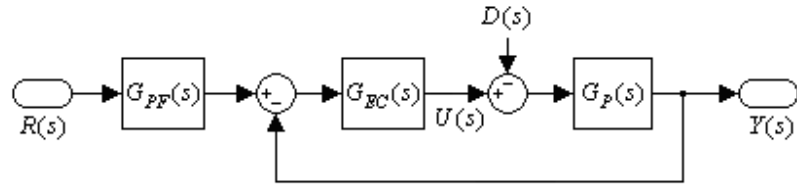
Figure 1: Block diagram of the equivalent ADRC controlled system

Redrawn from [27]

From the figure, it can be seen that the closed-loop system with ADRC can be represented by a unity feedback loop with a pre-filter. In the performance analyses in [27], the Bode diagram and the stability margins of the closed-loop system have been obtained. The unchanged values of the margins against the variations of system parameters demonstrate the notable robustness of ADRC against parameter uncertainties in the plant. Besides [27], a high order ADRC design was developed on a general transfer function form with zeros [28]. The design method was verified on a 3rd order plant with one zero and a

known time delay. However, this design approach did not consider the positive zeros for the transfer function form of an inherently unstable system. The physical system with positive zeros is still an unsolved problem for ADRC.

In the past twenty years, ADRC has been broadly employed in industry. The implementation of ADRC in motion control has been reported in [26]. ADRC is also employed in DC converters, chemical processes, and web tension control as presented in [29–31]. An application of ADRC solution to the control problem of a micro electro-mechanical system (MEMS) gyroscope is presented in [32]. The hardware implementations of ADRC for the MEMS gyroscope were introduced in [33, 34].

Those successful examples reported in the literature [25–34] have validated the effectiveness of ADRC and its great advantages over conventional control techniques such as PID control. ADRC is expected to be applied to more practical control problems in various fields including power systems.

1.4 Contribution of the thesis

In this thesis, a decentralized load frequency controller based on ADRC has been developed. It is the first time that ADRC was modified and applied to power systems. ADRC is chosen to solve the LFC problem of the power system because of its robustness against system uncertainties, its simple structure (with only two tuning parameters), and its effective tracking performance. Two types of power systems have been set up to test ADRC. The first

power system consists of three areas with non-reheat, reheat and hydraulic units in different areas. This system is used to check the feasibility and performance of ADRC solution for different generating units. The second power system has the same structure as the system presented in [23]. It is rebuilt in order to compare the performances between ADRC and the PI type controllers tuned via GALMI, an existing effective LFC solution. ADRC was simulated on the two types of power systems. The simulation verified the effectiveness of the controller. In addition, the robustness and stability of ADRC have been successfully proved through time-domain simulation results and frequency-domain analyses. The notable robustness of ADRC provides the controlled power systems with sufficient tolerances to the model and parameter uncertainties. The thesis provides strong theoretical support for the implementation of ADRC in the real-world LFC problem. Besides the contributions to the control of the power systems, the thesis also originally modified ADRC to control systems with zeros in the transfer functions.

1.5 Organization of the thesis

The thesis is organized as follows. Chapter II presents the model of the power generating system. The major components of the power system are discussed in this chapter. A Laplace transform representation of the decentralized area of the power system is also developed in Chapter II.

Chapter III introduces the design strategy of ADRC on an interconnected power system. First the application of ADRC to a second-order motion system is developed. Then

ADRC is generalized to an nth order plant with zeros in the transfer function representation of the plant. Finally the development of ADRC on the power system is presented in the chapter.

Chapter IV shows the simulation results of different types of disturbances on the two test power systems under the control of ADRC. In addition, both the parameter uncertainties on the non-reheat generating unit of the first test system and the model uncertainties of the second test system are discussed in this chapter in order to test the robustness of the designed controller.

Chapter V presents the frequency domain analyses of the system with ADRC. The closed-loop block diagram of the controlled system is obtained. The Bode diagrams and the stability margins are given for the two situations for the robustness test.

CHAPTER II

DYNAMICS OF THE POWER GENERATING SYSTEM

A comprehensive introduction to the dynamic models of general power systems can be found in [1]. In this chapter, the modeling of a typical power generating system, including the modeling of three types of generating units, the tie-line modeling and the modeling of parallel operation of interconnected areas will be introduced. A Laplace transform of a decentralized area of the power generating system will be derived for later frequency-domain analyses in Chapter V.

2.1 Power generating units

2.1.1 Turbines

A turbine unit in power systems is used to transform the natural energy, such as the energy from steam or water, into mechanical power (ΔP_m) that is supplied to the generator. In

LFC model, there are three kinds of commonly used turbines: non-reheat, reheat and hydraulic turbines, all of which can be modeled by transfer functions.

Non-reheat turbines are first-order units. A time delay (denoted by T_{ch}) occurs between switching the valve and producing the turbine torque. The transfer function can be of the non-reheat turbine is represented as

$$G_{NR}(s) = \frac{\Delta P_m(s)}{\Delta P_V(s)} = \frac{1}{T_{ch}s + 1}, \tag{1}$$

where ΔP_V is the valve/gate position change [1].

Reheat turbines are modeled as second-order units, since they have different stages due to high and low steam pressure. The transfer function can be represented as

$$G_R(s) = \frac{\Delta P_m(s)}{\Delta P_V(s)} = \frac{F_{hp}T_{rh}s + 1}{(T_{ch}s + 1)(T_{rh}s + 1)}, \tag{2}$$

where T_{rh} stands for the low pressure reheat time and F_{hp} represents the high pressure stage rating [2].

Hydraulic turbines are non-minimum phase units due to the water inertia. In the hydraulic turbine, the water pressure response is opposite to the gate position change at first and recovers after the transient response. Thus the transfer function of the hydraulic turbine is in the form of

$$G_H(s) = \frac{\Delta P_m(s)}{\Delta P_V(s)} = \frac{-T_w s + 1}{(T_w/2)s + 1}, \tag{3}$$

where T_w is the water starting time [1].

For stability concern, a transient droop compensation part in the governor is needed for the hydraulic turbine. The transfer function of the transient droop compensation part is given by

$$G_{TDC}(s) = \frac{T_R s + 1}{T_R (R_T/R)s + 1},$$

(4)

where T_R, R_T and R represent the reset time, temporary droop and permanent droop respectively [1].

2.1.2 Generators

A generator unit in power systems converts the mechanical power received from the turbine into electrical power. But for LFC, we focus on the rotor speed output (frequency of the power systems) of the generator instead of the energy transformation. Since electrical power is hard to store in large amounts, the balance has to be maintained between the generated power and the load demand.

Once a load change occurs, the mechanical power sent from the turbine will no longer match the electrical power generated by the generator. This error between the mechanical (ΔP_m) and electrical powers (ΔP_{el}) is integrated into the rotor speed deviation ($\Delta\omega_r$), which can be turned into the frequency bias (Δf) by multiplying by 2π. The relationship between ΔP_m and Δf is shown in Figure 2, where M is the inertia constant of the generator [1].
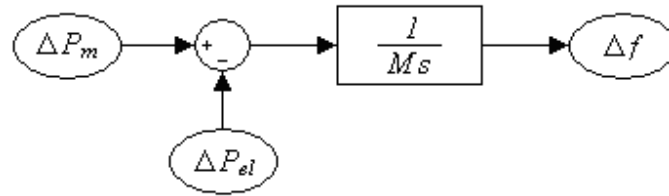
Figure 2: Block diagram of the generator

Redrawn from [1]

The power loads can be decomposed into resistive loads (ΔP_L), which remain constant when the rotor speed is changing, and motor loads that change with load speed [1]. If the mechanical power remains unchanged, the motor loads will compensate the load change at a rotor speed that is different from a scheduled value, which is shown in Figure 3, where D is the load damping constant [1].
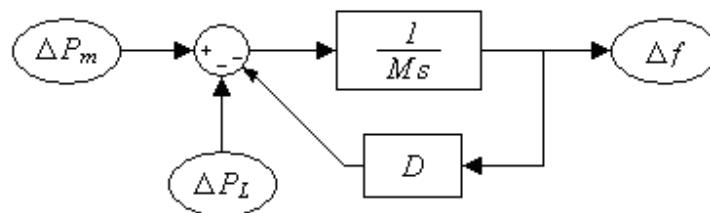
Figure 3: Block diagram of the generator with load damping effect

Redrawn from [1]

The reduced form of Figure 3 is shown in Figure 4, which is the generator model that we plan to use for the LFC design. The Laplace-transform representation of the block diagram in Figure 4 is

$$\Delta P_m(s) - \Delta P_L(s) = (Ms + D)\Delta F(s).$$
(5)
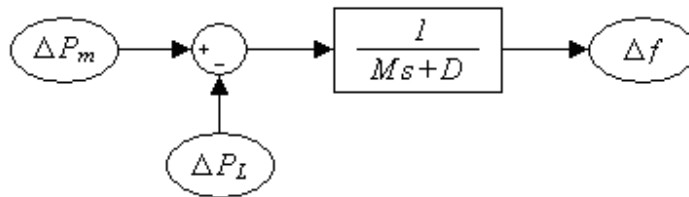
Figure 4: Reduced block diagram of the generator with the load damping effect

Redrawn from [1]

2.1.3 Governors

Governors are the units that are used in power systems to sense the frequency bias caused by the load change and cancel it by varying the inputs of the turbines. The schematic diagram of a speed governing unit is shown in Figure 5, where R is the speed regulation characteristic and T_g is the time constant of the governor [1]. If without load reference, when the load change occurs, part of the change will be compensated by the valve/gate adjustment while the rest of the change is represented in the form of frequency deviation. The goal of LFC is to regulate frequency deviation in the presence of varying active power load. Thus, the load reference setpoint can be used to adjust the valve/gate positions so that all the load change is canceled by the power generation rather than resulting in a frequency deviation.
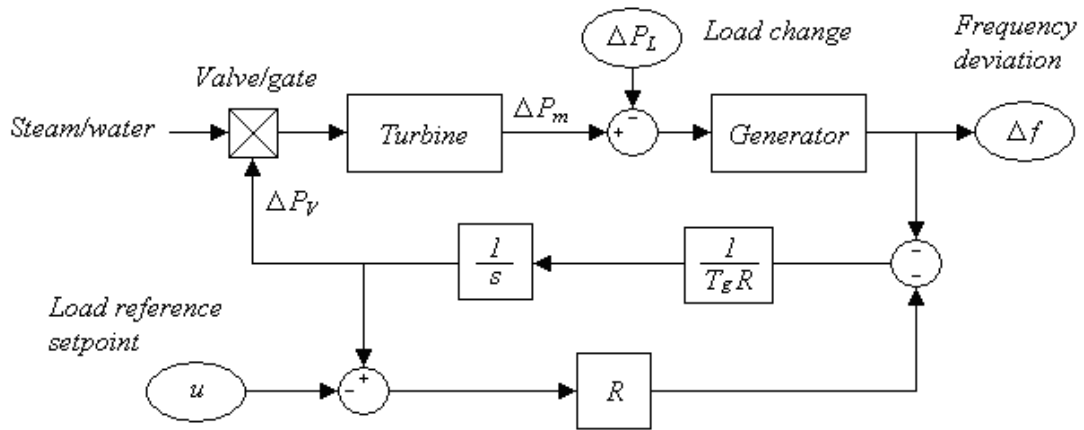
Figure 5: Schematic diagram of a speed governing unit

Redrawn and modified from [1]

The reduced form of Figure 5 is shown in Figure 6. The Laplace transform representation of the block diagram in Figure 6 is given by

$$U(s) - \frac{\Delta F(s)}{R} = (T_g s + 1)\Delta P_V(s).$$

(6)
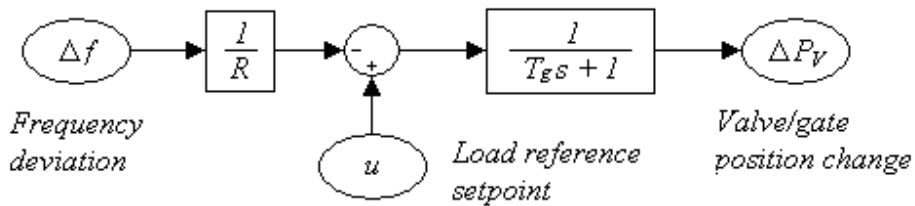
Figure 6: Reduced block diagram of the speed governing unit

Redrawn and modified from [1]

2.2 The interconnected power systems

2.2.1 Tie-lines

In an interconnected power system, different areas are connected with each other via tie-lines. When the frequencies in two areas are different, a power exchange occurs through the tie-line that connected the two areas. The tie-line connections can be modeled as shown in Figure 7. The Laplace transform representation of the block diagram in Figure 7 is given by

$$\Delta P_{tie\,ij}(s) = \frac{1}{s} T_{ij} \left(\Delta F_i(s) - \Delta F_j(s) \right), \qquad (7)$$

where ΔP_{tieij} is tie-line exchange power between areas i and j, and T_{ij} is the tie-line synchronizing torque coefficient between area i and j [1]. From Figure 7, we can see that the tie-line power error is the integral of the frequency difference between the two areas
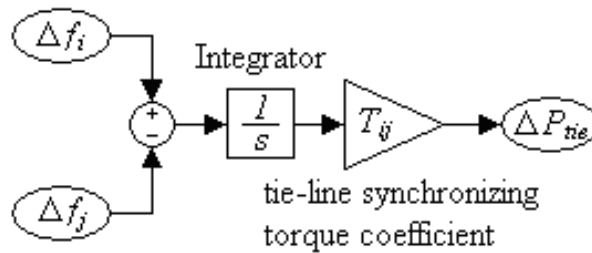
Figure 7: Block diagram of the tie-lines

2.2.2 Area control error

As discussed in Chapter I, the goals of LFC are not only to cancel frequency error in each area, but also to drive the tie-line power exchange according to schedule [1]. Since the tie-line power error is the integral of the frequency difference between each pair of areas, if we control frequency error back to zero, any steady state errors in the frequency of the system would result in tie-line power errors. Therefore we need to include the information of the tie-line power deviation into our control input. As a result, an area control error (ACE) is defined as

$$ACE_i = \sum_{j=1,\cdots,n, j \neq i} \Delta P_{tie\ ij} + B_i \Delta f_i, \text{ [1]} \tag{8}$$

where B_i is the frequency response characteristic for area i [1] and

$$B_i = D_i + \frac{1}{R_i}. \tag{9}$$

This ACE signal is used as the plant output of each power generating area. Driving ACEs in all areas to zeros will result in zeros for all frequency and tie-line power errors in the system [1].

2.2.3 Parallel operation

If there are several power generating units operating in parallel in the same area, an equivalent generator will be developed for simplicity. The equivalent generator inertia

constant (M_{eq}), load damping constant (D_{eq}) and frequency response characteristic (B_{eq}) can

be represented as follows.

$$M_{eq} = \sum_{i=1,\cdots,n} M_i \tag{10}$$

$$D_{eq} = \sum_{i=1,\cdots,n} D_i \tag{11}$$

$$B_{eq} = \sum_{i=1,\cdots,n} \frac{1}{R_i} + \sum_{i=1,\cdots,n} D_i \,. \tag{12}$$

2.3 Dynamic model of one-area power generating units

With the power generating units and the tie-line connections of interconnected areas

introduced in Sections II.1 and II.2, a complete form of one-area power generating unit can

be constructed as Figure 8.
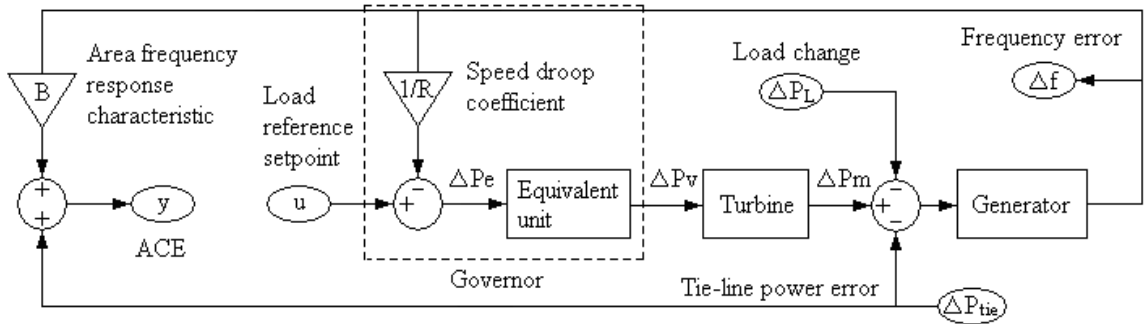
Figure 8: Schematic of one-area power generating unit

In Figure 8, there are three inputs, which are the controller input *U(s)*, load

disturbance *ΔP_L(s)*, and tie-line power error *ΔP_tie(s)*, one ACE output *Y(s)* and one generator

output Δf. The term ΔP_e is not in Figure 5 because it does not have a physical meaning. We note the input of the equivalent unit in the governor as ΔP_e for simplicity when developing the Laplace transform of the one-area power generating plant.

2.4 The Laplace transform model of one-area power generating plant

We consider the plant shown in Figure 8. The relationships between the inputs and output in Figure 8 can be described as

$$U(s) - \frac{1}{R}\Delta F(s) = \Delta P_e(s),\tag{13}$$

$$G_{EU}(s)\Delta P_e(s) = \Delta P_V(s),\tag{14}$$

$$G_{Tur}(s)\Delta P_V(s) = \Delta P_m(s),\tag{15}$$

$$(\Delta P_m(s) - \Delta P_L(s) - \Delta P_{tie}(s))G_{Gen}(s) = \Delta F(s),\tag{16}$$

$$Y(s) = B\Delta F(s) + \Delta P_{tie}(s),\tag{17}$$

where $G_{EU}(s)$, $G_{Tur}(s)$ and $G_{Gen}(s)$ are the transfer functions for the equivalent unit, the turbine and the generator respectively.

For the ease of transfer function development, let the transfer function from $\Delta P_e(s)$ that we defined in Figure 8 to the mechanical power deviation $\Delta P_m(s)$ be $G_{ET}(s) = Num_{ET}(s) / Den_{ET}(s)$, where $Num_{ET}(s)$ and $Den_{ET}(s)$ are the numerator and denominator of $G_{ET}(s)$ respectively. The representation of $Num_{ET}(s)$ and $Den_{ET}(s)$ may vary

from different generating units. For the non-reheat unit, the combined transfer function of the equivalent unit in governor $G_{ET}(s)$ can be expressed as

$$G_{ET}(s) = \frac{Num_{ET}(s)}{Den_{ET}(s)} = \frac{1}{(T_g s + 1)(T_{ch} s + 1)}. \tag{18}$$

For the reheat unit, we have

$$G_{ET}(s) = \frac{Num_{ET}(s)}{Den_{ET}(s)} = \frac{F_{hp} T_{rh} s + 1}{(T_g s + 1)(T_{ch} s + 1)(T_{rh} s + 1)}. \tag{19}$$

For the hydraulic unit, we have

$$G_{ET}(s) = \frac{Num_{ET}(s)}{Den_{ET}(s)} = \frac{(T_R s + 1)(-T_w s + 1)}{(T_g s + 1)\left[T_R (R_T / R)s + 1\right]\left[(T_w / 2)s + 1\right]}. \tag{20}$$

Define the transfer function of the generator as

$$G_{Gen}(s) = \frac{1}{Den_M(s)} = \frac{1}{Ms + D}, \tag{21}$$

where $Den_M(s)$ represents the denominator of $G_{Gen}(s)$. The Laplace transform of the one-area power generating plant can be simplified as

$$Y(s) = G_P(s)U(s) + G_D(s)\Delta P_L(s) + G_{tie}(s)\Delta P_{tie}(s), \tag{22}$$

where

$$G_P(s) = \frac{RBNum_{ET}(s)}{Num_{ET}(s) + RDen_{ET}(s)Den_M(s)}, \tag{23}$$

$$G_D(s) = \frac{-RBDen_{ET}(s)}{Num_{ET}(s) + RDen_{ET}(s)Den_M(s)}, \qquad (24)$$

$$G_{tie}(s) = \frac{Num_{ET}(s) + RDen_{ET}(s)Den_M(s) - RBDen_{ET}(s)}{Num_{ET}(s) + RDen_{ET}(s)Den_M(s)}. \qquad (25)$$

2.5 Summary of the chapter

The modeling of each part in the power generating unit is discussed in this chapter, followed by the Laplace transform development of the decentralized power generating area. The control objective of the LFC problem has been specified as to drive the ACE in each area back to zero. This chapter has laid the groundwork for both the controller design and the constructions of the power test systems.

CHAPTER III

ON THE DESIGN OF ACTIVE DISTURBANCE REJECTION

CONTROLLER

In the model of the power system developed in last chapter, the parameter values in the model fluctuate depending on system and power flow conditions which change almost every minute. Therefore, dealing with the parameter uncertainties will be an essential factor to choose a control solution to the load frequency control (LFC) problem. After comparing the existing advanced controllers introduced in Chapter I, we selected active disturbance rejection controller (ADRC) as the LFC. In this chapter, the design strategies of ADRC are developed on a general transfer function model of a physical system. Both time-domain and Laplace-domain representations of ADRC are derived in this chapter.

3.1 The idea of active disturbance rejection control

Although we aim to develop ADRC for the high-order power plant, we will introduce the design idea of ADRC on a second order plant for the convenience of explanation.

We consider a motion system that can be described as

$$\ddot{y}(t) + a_1 \dot{y}(t) + a_2 y(t) = bu(t) + w(t), \tag{26}$$

where $u(t)$ is the input force of the system, $y(t)$ is the position output, $w(t)$ represents the external disturbance of the system, a_1, a_2 and b are the coefficients of the differential equation. ADRC design approaches can be summarized as four steps.

Step 1: Reform the plant

(26) can be rewritten as

$$\ddot{y}(t) = bu(t) + w(t) - a_1 \dot{y}(t) - a_2 y(t). \tag{27}$$

As introduced in [26], the partial information of the plant $-a_1 \dot{y}(t) - a_2 y(t)$ can be referred to as internal dynamics. The internal dynamics of the system combined with the external disturbance $w(t)$ can form a generalized disturbance, denoted as $d(t)$. Then (27) can be rewritten as

$$\ddot{y}(t) = bu(t) + d(t). \tag{28}$$

The generalized disturbance contains both the unknown external disturbance and the uncertainties in internal dynamics. So as the generalized disturbance is observed and cancelled by ADRC, the uncertainties included in the disturbance will be canceled as well.

In this way of reforming, all second-order linear systems with different values of a_1 and a_2 can be classified in one category. The systems in this category have two common characteristics: one is the order of the plant, and the other is the high frequency gain b [25]. We will find out that those two characteristics are the essential information required for ADRC design instead of the accurate plant model.

Step 2: Estimate the generalized disturbance

As discussed in Step 1, we need to cancel the generalized disturbance after reforming the plant. One way is to obtain the dynamic model of the disturbance and cancel it theoretically. But this idea does not match our original intention to set up a controller with little information required from the plant. Moreover, the external disturbance could be random and cannot be modeled. Thus we have to use another way to cancel the generalized disturbance rather than to cancel it theoretically. A practical method is to treat the generalized disturbance as an extra state of the system and use an observer to estimate its value. This observer is known as an extended state observer (ESO) [25].

The state space model of (28) is

$$\dot{x} = Ax + Bu + E\dot{d}$$
$$y = Cx$$

(29)

In (29), $x = \begin{bmatrix} x_1 \\ x_2 \\ x_3 \end{bmatrix}$, where $x_1 = y$, $x_2 = \dot{y}$, $x_3 = d$, $A = \begin{bmatrix} 0 & 1 & 0 \\ 0 & 0 & 1 \\ 0 & 0 & 0 \end{bmatrix}$, $B = \begin{bmatrix} 0 \\ b \\ 0 \end{bmatrix}$, $E = \begin{bmatrix} 0 \\ 0 \\ 1 \end{bmatrix}$, and

$C = \begin{bmatrix} 1 & 0 & 0 \end{bmatrix}$. It is assumed that d has local Lipschitz continuity and $\dot{d}$ is bounded within

domain of interests [35]. From (29), the ESO is derived as

$$\dot{z} = Az + Bu + L(y - \hat{y})$$
$$\hat{y} = Cz$$, [25]

(30)

where $z = \begin{bmatrix} z_1 & z_2 & z_3 \end{bmatrix}^T$ is the estimated state vector of x, and $\hat{y}$ is the estimated system

output y. L is the ESO gain vector and $L = \begin{bmatrix} \beta_1 & \beta_2 & \beta_3 \end{bmatrix}^T$. To locate all the eigenvalues of the

ESO at $-\omega_O$, the values of the elements of the vector L are chosen as

$$\beta_i = \binom{3}{i} \cdot \omega_O^i, \ i = 1, 2, 3 . \ [25]$$

(31)

With a well tuned ESO, z_i will track x_i closely. Then we will have

$$z_3 \approx x_3 = d .$$

(32)

From (32), this generalized disturbance $d(t)$ can be approximately removed by the

time domain estimated value z_3.

Step 3: Simplify the plant

With the control law

$$u = \frac{u_0 - z_3}{b}, \text{[25]}$$ (33)

the system described in (28) becomes

$$\begin{aligned}
\ddot{y} &= b\frac{u_0 - z_3}{b} + d \\
&\approx (u_0 - d) + d \quad . \\
&= u_0
\end{aligned}$$ (34)

From (34), we can see that with accurate estimation of ESO, the second-order LTI system could be simplified into a pure integral plant approximately. Then a classic state feedback control law could be used to drive the plant output y to a desired reference signal.

Step 4: Design a control law for the simplified plant

The state feedback control law for the simplified plant $\ddot{y} \approx u_0$ is chosen as

$$u_0 = k_1(r - z_1) - k_2 z_2 . \text{[25]}$$ (35)

From (30), z_1 will track y, and z_2 will track $\dot{y}$. Then substituting u_0 in $\ddot{y} \approx u_0$ with (35) yields

$$\ddot{y} = k_1 r - k_1 y - k_2 \dot{y} .$$ (36)

The Laplace transform of (36) is

$$s^2 Y(s) + k_2 s Y(s) + k_1 Y(s) = k_1 R(s) . \tag{37}$$

The closed-loop transfer function from the reference signal to the position output is

$$G_{cl}(s) = \frac{Y(s)}{R(s)} = \frac{k_1}{s^2 + k_2 s + k_1} . \tag{38}$$

Let $k_1 = \omega_C^2$ and $k_2 = 2\omega_C$ [25]. We will have

$$G_{cl}(s) = \frac{\omega_C^2}{s^2 + 2\omega_C s + \omega_C^2} = \frac{\omega_C^2}{(s + \omega_C)^2} , \tag{39}$$

where ω_C represents the bandwidth of the controller. With the increase of the ω_C, the tracking speed of the output of ADRC controlled system will increase as well while the tracking error and overshoot percentage of the output will be decreased. The detailed information about the relationship between the parameters ω_C and ω_O and the control performance can be found in [34].

3.2 ADRC design for a general-form plant

In the Laplace domain, a plant with disturbance can be represented as

$$Y(s) = G_p(s) \cdot U(s) + W(s), \tag{40}$$

where $U(s)$ and $Y(s)$ are the input and output respectively, $W(s)$ is the generalized disturbance. In (40), the general transfer function of a physical plant $G_p(s)$ can be represented as

$$\frac{Y(s)}{U(s)} = G_P(s) = \frac{b_m s^m + b_{m-1} s^{m-1} + \cdots + b_1 s + b_0}{a_n s^n + a_{n-1} s^{n-1} + \cdots + a_1 s + a_0}, \quad n \geq m, \tag{41}$$

where a_i and b_j ($i = 1, \ldots, n, j = 1, \ldots, m$) are the coefficients of the transfer function.

From (28), we can infer that the basic idea of ADRC design is based on the transfer function of the plant without zeros. Thus in order to implement ADRC for the system represented by (40), we need to develop an equivalent model of (41) so that the transfer function only has poles. The error between the two models can be included into the generalized disturbance term.

In order to develop the non-zero equivalent model of (41), the following polynomial long division is conducted on $1 / G_p(s)$.

$$\frac{1}{G_P(s)} = \frac{a_n s^n + a_{n-1} s^{n-1} + \cdots + a_1 s + a_0}{b_m s^m + b_{m-1} s^{m-1} + \cdots + b_1 s + b_0} \quad (n \geq m)$$
$$= c_{n-m} s^{n-m} + c_{n-m-1} s^{n-m-1} + \cdots + c_1 s + c_0 + G_{left}(s) \tag{42}$$

In (42), c_i ($i = 0, \ldots, n - m$) are coefficients of the polynomial division result, and the $G_{left}(s)$ is a remainder, which can be represented by

$$G_{left}(s) = \frac{d_{m-1} s^{m-1} + d_{m-2} s^{m-2} + \cdots + d_1 s + d_0}{b_m s^m + b_{m-1} s^{m-1} + \cdots + b_1 s + b_0}. \tag{43}$$

In (43), d_j ($j = 0, \ldots, m - 1$) are coefficients of the numerator of the remainder. Substituting (42) into (40), we have

$$\left[c_{n-m} s^{n-m} + c_{n-m-1} s^{n-m-1} + \cdots + c_1 s + c_0 + G_{left}(s) \right] Y(s) = U(s) + W'(s), \tag{44}$$

where $W'(s) = W(s) / G_p$. (44) can be rewritten as

$$c_{n-m}s^{n-m}Y(s) = U(s) - \left[c_{n-m-1}s^{n-m-1} + \cdots + c_1 s + c_0 + G_{left}(s) \right] Y(s) + W'(s). \quad (45)$$

Finally we have

$$s^{n-m}Y(s) = \frac{1}{c_{n-m}}U(s) + D(s), \quad (46)$$

where

$$D(s) = -\frac{1}{c_{n-m}}\left[c_{n-m-1}s^{n-m-1} + \cdots + c_1 s + c_0 + G_{left}(s) \right] Y(s) + \frac{1}{c_{n-m}}W'(s). \quad (47)$$

From (42), it can be seen that

$$c_{n-m} = \frac{a_n}{b_m}. \quad (48)$$

However, it is difficult to get the expressions of the other coefficients in (42) and (43). Fortunately from the development process of ADRC, $D(s)$ is treated as the generalized disturbance and will be estimated in time domain so that we do not actually need the exact expressions for the c_i and d_j ($i = 0, \dots , n - m, j = 0, \dots, m - 1$) in (42) and (43).

From (46), we can see that the two characteristics (relative order between input and output and controller gain) have been extracted from the plant by modifying the Laplace transform. Instead of using the order of the plant n, we utilize the relative order $n - m$ as the order of the controlled system. The high frequency gain (denoted as b) is still the ratio

between the coefficients of the highest-order terms of the numerator and the denominator.

After obtaining the equivalent order and the high frequency gain, (46) can rewritten as

$$s^{n-m}Y(s) = bU(s) + D(s), \tag{49}$$

where $b = 1 / c_{n-m}$.

Now we extend ADRC design approach discussed in Section III.1 to $n - m$ dimensions. The state space model of (49) is

$$
\begin{aligned}
sX(s) &= AX(s) + BU(s) + EsD(s) \\
Y(s) &= CX(s)
\end{aligned}, \tag{50}
$$

where $X(s) = \begin{bmatrix} X_1(s) \\ X_2(s) \\ \vdots \\ X_{n-m}(s) \end{bmatrix}_{(n-m)}$, $A = \begin{bmatrix} 0 & 1 & 0 & \cdots & 0 \\ 0 & \ddots & 1 & \ddots & \vdots \\ \vdots & \ddots & 0 & \ddots & 0 \\ \vdots & \ddots & \ddots & \ddots & 1 \\ 0 & 0 & \cdots & \cdots & 0 \end{bmatrix}_{(n-m)\times(n-m)}$, $B = \begin{bmatrix} 0 \\ \vdots \\ 0 \\ b \\ 0 \end{bmatrix}_{(n-m)}$, $E = \begin{bmatrix} 0 \\ \vdots \\ 0 \\ 0 \\ 1 \end{bmatrix}_{(n-m)}$,

$C = \begin{bmatrix} 1 & 0 & \cdots & 0 \end{bmatrix}_{(n-m)}$. In (49), $D(s)$ is still required to have local Lipschitz continuity and $sD(s)$ is bounded with domain of interests [35]. The ESO of the plant is

$$
\begin{aligned}
sZ(s) &= AZ(s) + BU(s) + L(Y(s) - \hat{Y}(s)) \\
\hat{Y}(s) &= CZ(s)
\end{aligned}, \tag{51}
$$

where $Z(s) = \begin{bmatrix} Z_1(s) & Z_2(s) & \cdots & Z_{n-m}(s) \end{bmatrix}^T_{(n-m)}$ and $L = \begin{bmatrix} \beta_1 & \beta_2 & \cdots & \beta_{(n-m)} \end{bmatrix}^T_{(n-m)}$. In order to locate all the eigenvalues of the ESO to $-\omega_O$, the observer gains are chosen as

$$\beta_i = \binom{n-m}{i} \cdot \omega_O^i, \ i = 1, \cdots, n-m.$$ (52)

With a well tuned ESO, $Z_i(s)$ will be able to estimate the value of $X_i(s)$ closely $(i = 1, \ldots, n - m)$. Then we have

$$Z_{n-m}(s) = \hat{D}(s) \approx D(s).$$ (53)

The control law

$$U(s) = (U_0(s) - Z_{n-m}(s))/b,$$ (54)

will reduce (49) to a pure integral plant, i.e.,

$$\begin{aligned} s^{n-m}Y(s) &= b \cdot (U_0(s) - Z_{n-m}(s))/b + D(s) \\ &= U_0(s) - \hat{D}(s) + D(s) \approx U_0(s) \end{aligned}.$$ (55)

The control law for the pure integral plant is

$$U_0(s) = k_1(R(s) - Z_1(s)) - k_2 Z_2(s) - \cdots - k_{n-m-1} Z_{n-m-1}(s).$$ (56)

To further simplify the tuning process, all the closed-loop poles of the PD controller are set to $-\omega_C$. Then the controller gains in (56) have to be selected as

$$k_i = \binom{n-m-1}{n-m-i} \cdot \omega_C^{n-m-i}, \ i = 1, \cdots, n-m-1.$$ (57)

3.3 The design solution for the plant with positive zeros

In ADRC design, the generalized disturbance $d(t)$ is required to have local Lipschitz continuity and $\dot{d}(t)$ has to be bounded with the domain of interests for stability concern. As we design an ADRC for a physical plant (41) with any order, we will have to include a $\mathcal{L}^{-1}[G_{left}(s)Y(s)]$ term in $d(t)$, which should also be bounded. The bounded condition for $d(t)$ requires $G_{left}(s)$ to have all negative poles, which demands that the transfer function $G_p(s)$ should have all negative zeros since $G_{left}(s)$ is derived from $1 / G_p(s)$. Thus, if there are any positive zeros in $G_p(s)$, they should be canceled before designing an ADRC for the system. Specifically, for the hydraulic unit in the power system to be controlled, there is a positive zero $s = 1 / T_w$ in the Laplace transform of the decentralized plant. To apply ADRC to this unit, a compensator with a transfer function of $1 / (-T_w s + 1)$ is needed to cancel the positive zero in the plant.

3.4 Summary of the chapter

In this chapter, the design process of ADRC has been divided into four steps. First, ADRC was implemented on a second-order system. Then it has been extended to a system with a general-form transfer function of any order. Both time-domain and Laplace-domain representation of ADRC are developed in this chapter. The design solution to the plant with positive zeros has also been discussed at the end of the chapter.

CHAPTER IV

POWER SYSTEM SIMULATION

In this chapter, ADRC is applied to two kinds of decentralized power systems, which are constructed to test the effectiveness of the controller. The first test system consists of three different types of generating units, which include reheat, non-reheat and hydraulic turbines, generators, and governors. In order to test the robustness of ADRC, it is assumed that all of the parameters in the non-reheat unit of the system have 20% floating rates from their nominal values. The second test system was proposed in the literature [23]. It is composed of nine similar non-reheat units that are evenly distributed in three areas. This test system is used to compare the control performances between the GALMI tuned PI controller and ADRC. The stability and robustness of ADRC are tested under an extreme condition that one generating unit fails to operate in the interconnected power system, where all of the areas are connected with each other through tie-lines. All the simulations in this thesis have been completed using MATLAB/Simulink®.

4.1 On the three-area interconnected power system with different generating units

The first test system consists of three different decentralized areas, which are connected to each other through tie-lines. Each area has three major components, which are turbine, govener, and generator. Non-reheat, reheat and hydraulic turbine units are distributed in the three areas respectively. ADRC controlled interconnected power system is shown in Figure 9. The parameters of the system are obtained from [1, 2], and listed in Table 1. The definitions of the parameters have already been given in Chapter II.
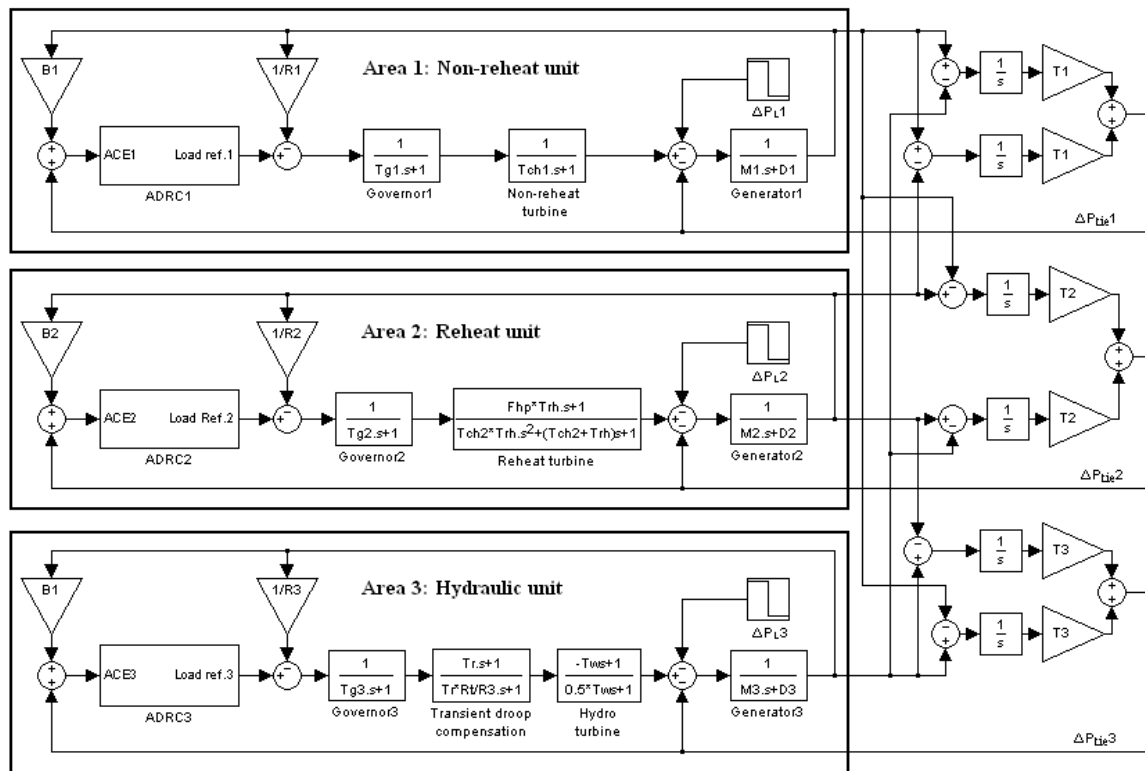

Figure 9: Three-area power system with different units

Table 1: System parameters of the power plant [1, 2]

Non-reheat		Reheat		Hydraulic	
M1 (p.u. sec.)*	`10±20%`	*M2 (p.u. sec.)*	`10.0`	*M3 (p.u. sec.)*	`6.0`
D1 (p.u./Hz)	`1±20%`	*D2 (p.u./Hz)*	`1.0`	*D3 (p.u./Hz)*	`1.0`
Tch1 (sec.)	`0.3±20%`	*Tch2 (sec.)*	`0.3`	*Tg3 (sec.)*	`0.2`
Tg1 (sec.)	`0.1±20%`	*Fhp*	`0.3`	*Tr (sec.)*	`5.0`
R1 (Hz/p.u.)	`0.05∓20%`	*Trh (sec.)*	`7.0`	*Rt (Hz/p.u.)*	`0.38`
T1 (p.u./rad.)	`22.6±20%`	*Tg2 (sec.)*	`0.2`	*R3 (Hz/p.u.)*	`0.05`
		R2 (Hz/p.u.)	`0.05`	*Tw (sec.)*	`1.0`
		T2 (p.u./rad.)	`22.6`	*T3 (p.u./rad.)*	`22.6`

*: p.u. represents per unit.

For each decentralized area in Figure 9, an ADRC is designed based on the transfer function $G_P(s)$ in (23), whose parameter values are listed in Table 1. The transfer functions of the non-reheat ($G_{PN}(s)$), reheat ($G_{PR}(s)$) and hydraulic ($G_{PH}(s)$) units are given by

$$G_{PN}(s) = \frac{1.05}{0.015s^3 + 0.2015s^2 + 0.52s + 1.05}, \tag{58}$$

$$G_{PR}(s) = \frac{2.205\ s + 1.05}{0.21\ s^4 + 1.801\ s^3 + 3.928\ s^2 + 2.975\ s + 1.05}, \tag{59}$$

$$G_{PH}(s) = \frac{-5.25\ s^2 + 4.2\ s + 1.05}{1.14\ s^4 + 8.2\ s^3 + 7.945\ s^2 + 6.235\ s + 1.05}. \tag{60}$$

From the equation above, we can see that the transfer function of hydraulic unit has a positive zero, which can bring instability to the system. Therefore, before we apply ADRC to the area with the hydraulic unit, we will have to design a compensator to the area so as to cancel out the positive zero. With the compensator designed as $1 / (-s + 1)$, the transfer function of the hydraulic unit becomes

$$G_{PH\_C}(s) = \frac{5.25\ s + 1.05}{1.14\ s^4 + 8.2\ s^3 + 7.945\ s^2 + 6.235\ s + 1.05}. \tag{61}$$

According to the discussions in Chapter III, ADRC (including its ESO) for area 1 can be designed and represented by the following equations.

$$sZ(s) = (A - LC)Z(s) + BU(s) + LY(s), \tag{62}$$

$$U_0(s) = k_1(R(s) - Z_1(s)) - k_2 Z_2(s) - k_3 Z_3(s), \tag{63}$$

$$U(s) = \frac{U_0(s) - Z_4(s)}{b}, \tag{64}$$

where $Z(s) = \begin{bmatrix} Z_1(s) \\ Z_2(s) \\ Z_3(s) \\ Z_4(s) \end{bmatrix}$, $A = \begin{bmatrix} 0 & 1 & 0 & 0 \\ 0 & 0 & 1 & 0 \\ 0 & 0 & 0 & 1 \\ 0 & 0 & 0 & 0 \end{bmatrix}$, $B = \begin{bmatrix} 0 \\ 0 \\ b \\ 0 \end{bmatrix}$, $C = \begin{bmatrix} 1 & 0 & 0 & 0 \end{bmatrix}$, $L = \begin{bmatrix} 4\omega_O \\ 6\omega_O^2 \\ 4\omega_O^3 \\ \omega_O^4 \end{bmatrix}$, $k_1 = \omega_C^3$,

$k_2 = 3\omega_C^2$, $k_3 = 3\omega_C$. ADRCs for the other two areas have the similar structure to ADRC for area 1. The design parameters of ADRCs in different areas are given in Table 2.

Table 2: ADRC parameters of the first test system

	Order of ESO	ω_C	ω_O	b
Area 1	4	4	20	70.0
Area 2	4	4	20	10.5
Area 3	4	4	20	4.6

The performance of ADRC is tested for three cases of system parameters. A 0.1 *p.u.* (per unit) step load change is applied to the three different areas at $t = 2$, 7, and 12 seconds

respectively. In the different cases, the parameter values of the non-reheat unit in area 1 will have different values. In the following three cases, the controller parameter values of ADRC remain unchanged. The parameter values are same as the ones listed in Table 2.

In case 1, the parameters of the non-reheat unit in area 1 are chosen to have nominal values. The effectiveness of ADRC will be tested in this case by simulating the closed-loop control system in Figure 9. In our simulation results, area 1 is denoted as the area with non-reheat unit (or non-reheat), area 2 is denoted as the area with reheat unit (or reheat), and area 3 is denoted as the area with hydraulic unit (or hydraulic). The system responses for three different areas are shown in Figures 10, 11, and 12. Figure 10 illustrates the Area Control Error (ACE) outputs of the three different areas. Figure 11 illustrates the frequency errors (Δf) of the three different areas. Figure 12 shows the tie-line power errors of the three areas. From the simulation results, we can see that the ACEs, the frequency errors, and tie-line power deviations have been driven to zero by ADRC in the presences of power load changes. The average settling time in the system responses is around 3 seconds. From the three figures, we can also see that the responses of the area with hydraulic unit have biggest overshoot percentages compared to the other areas. We believe this is because the hydraulic unit is inherently unstable. The instability could cause the big oscillation during the transient period.
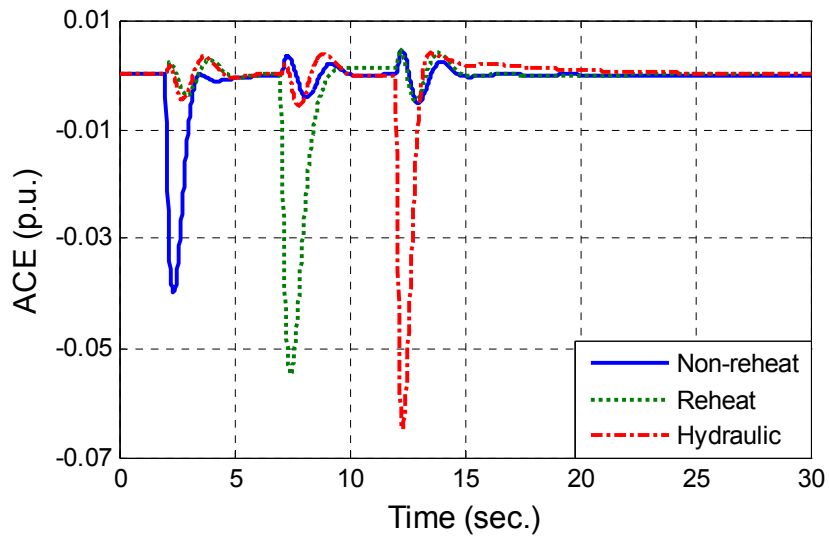
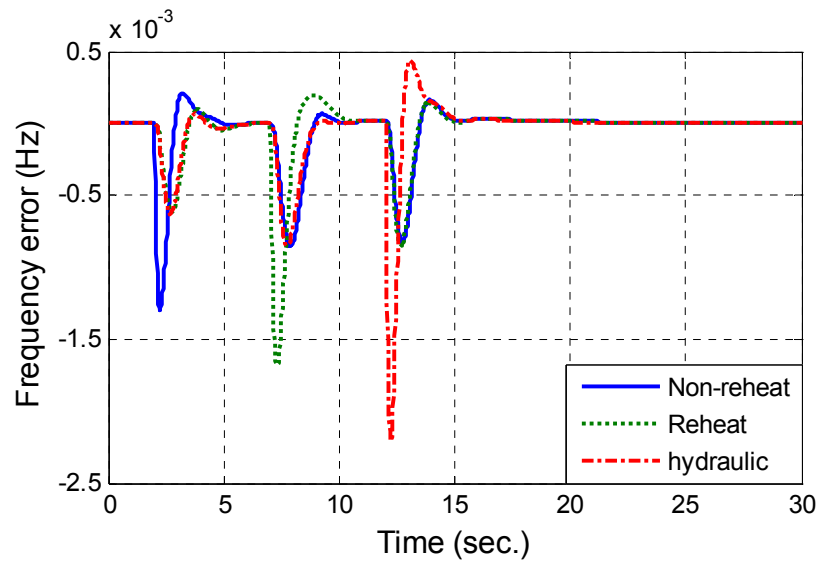*Figure 10: ACEs of the three-area power systems*

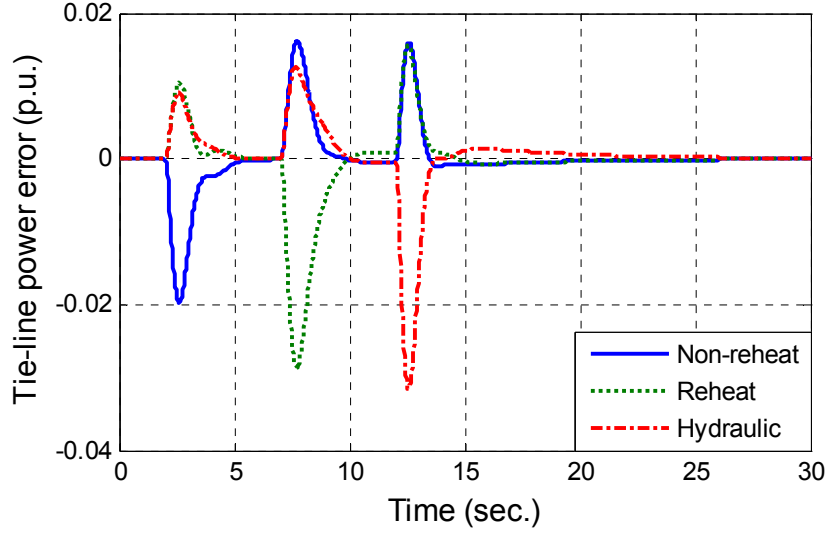*Figure 11: Frequency errors of the three-area power systems*

Figure 12: Tie-line power errors of the three-area power systems

In case 2, in order to test the robustness of ADRC, the variations of all of the parameters (M_1, D_1, T_{ch1}, T_{g1}, R_1, and T_1) of the non-reheat unit in the first area are assumed to be −20% and 20% of their nominal values respectively. However, the controller parameters of ADRC are not changed with the variations of the system parameters. The responses of area 1 are shown in Figures 13, 14 and 15. Figure 13 illustrates the ACE outputs of area 1 with the variant parameter values for the non-reheat unit. Figure 14 illustrates the frequency errors of area 1 with the variant parameter values for the non-reheat unit. Figure 15 shows the tie-line power errors of area 1 with the variant parameter values for the non-reheat unit. From the simulation results, we can see that despite such large parameter variations, the system responses do not show notable differences from the results in Figures 10, 11, and 12. Therefore the simulation results demonstrate the robustness of ADRC against system parameter variations. If we change the system parameters for reheat and hydraulic units, the same conclusion is obtained since the model for each area is similar to the others.
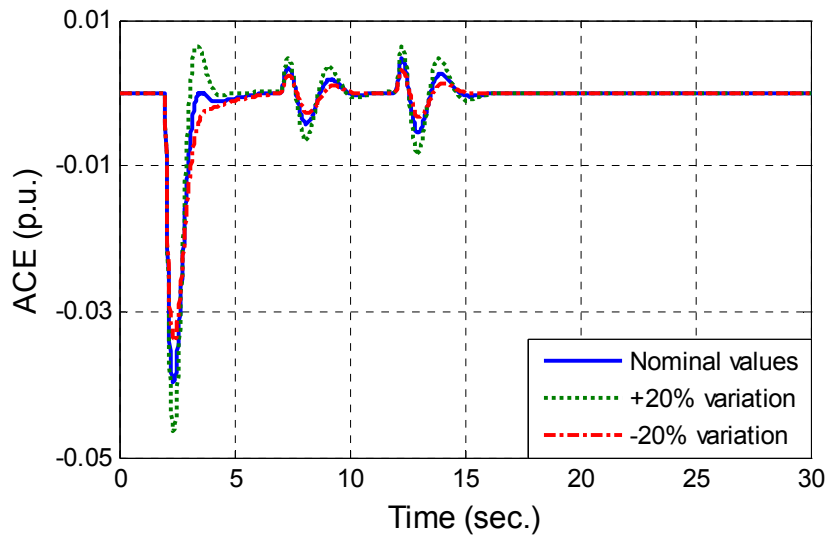
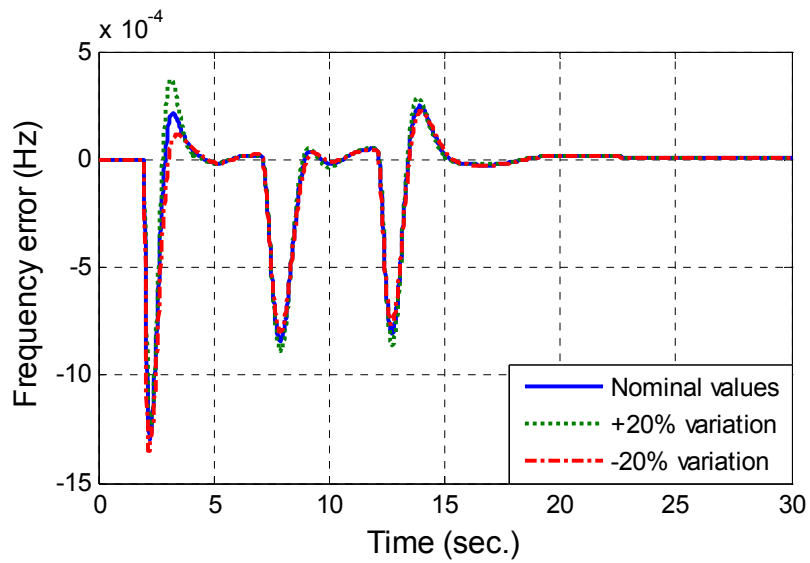*Figure 13: ACEs of area 1 with variant parameter values for non-heat unit*

Figure 14: Frequency errors of area 1 with variant parameter values for non-reheat
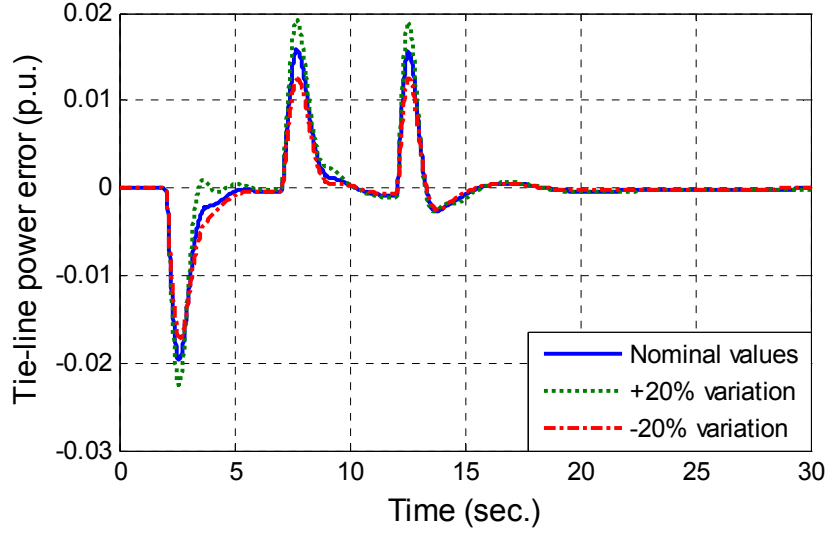
unit

Figure 15: Tie-line power errors of area 1 with variant parameter values for non-reheat unit

4.2 On the three-area non-reheat test system

The second test system also has three areas. Each area has three parallel-operating generating units that are owned by different generation companies (GenCos). Every generating unit has a non-reheat turbine unit, a generator, and a governor. The schematic diagram of the system is shown in Figure 16, where the three areas are connected with each other through tie-lines. In this figure, ΔP_{L1}, ΔP_{L2}, and ΔP_{L3} are power load changes added to the three areas. The dynamic model of area 1 is shown in Figure 17, which is similar to the model in [23], where a GALMI tuned PI controller was proposed. This GALMI tuned PI control method is very popular in current power industry. We choose a system model similar to the one in [23] for the comparison of the performances between the GALMI tuned PI controller in [23] and ADRC controller in this thesis.

The tie-line synchronizing coefficients between any two areas are $T_{12} = 0.2$ *p.u./rad.*, $T_{23} = 0.12$ *p.u./rad.* and $T_{13} = 0.25$ *p.u./rad.*. The ramp rate factor that is used to describe the rate of change in the power plant output is given as

$$\alpha = \frac{Ramprate \times 5\,min}{Regulation\ requirement}, \tag{65}$$

in which the regulation requirement for each area is 100 *MW*. The ramp rate and all the other parameters of the system in Figure 17 are given in Table 3.
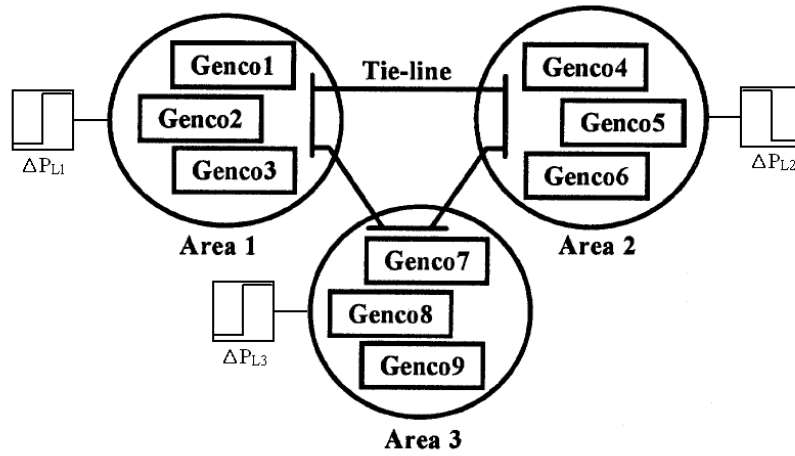

Figure 16: Schematic diagram of the three-area nine-unit power system
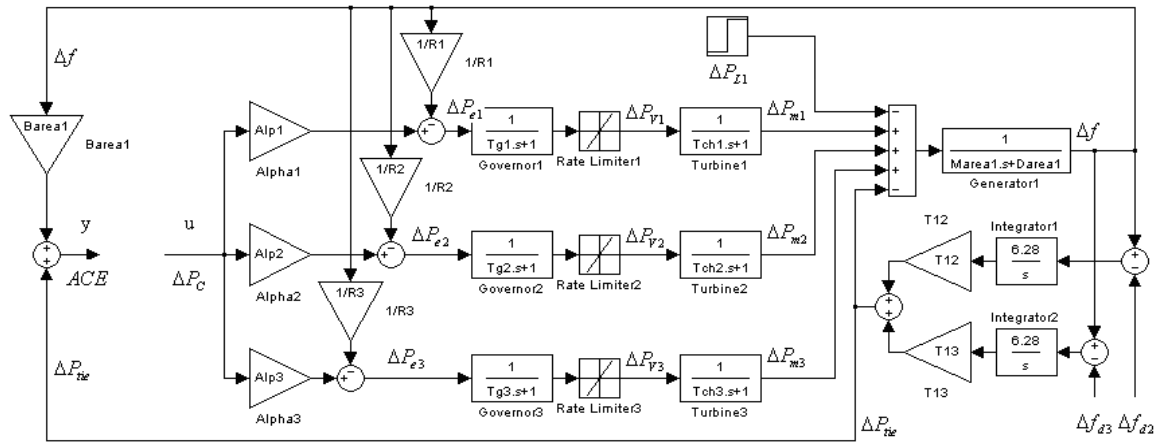
Redrawn from [23]

Figure 17: Dynamic model of one area for the second test system

Redrawn from [23]

Table 3: Generating unit parameters [23]

Parameters	GenCo								
MVA base (*1000MW*)	1	2	3	4	5	6	7	8	9
D (p.u./Hz)	0.0150	0.0140	0.0150	0.0160	0.0140	0.0140	0.0150	0.0160	0.0150
M (p.u. sec.)	0.1667	0.1200	0.2000	0.2017	0.1500	0.1960	0.1247	0.1667	0.1870
T_{ch} *(sec.)*	0.4	0.36	0.42	0.44	0.32	0.40	0.30	0.40	0.41
T_g *(sec.)*	0.08	0.06	0.07	0.06	0.06	0.08	0.07	0.07	0.08
R (Hz/p.u.)	3.00	3.00	3.30	2.7273	2.6667	2.50	2.8235	3.00	2.9412
B (p.u./Hz)	0.3483	0.3473	0.3180	0.3827	0.3890	0.4140	0.3692	0.3493	0.3550
α	0.4	0.4	0.2	0.6	0	0.4	0	0.5	0.5
Ramp rate (MW/min.)	8	8	4	12	0	8	0	10	10

ADRC based controller is implemented on each area of the system in Figure 17. The controller parameters for both ADRC and the GALMI are listed in Table 4 and Table 5 respectively. In this section, the performance of ADRC is compared with that of the GALMI

tuned PI controller in [23] for three cases of load changes. Some preliminary results about the comparison study were reported in [36].

Table 4: ADRC parameters of the second test system

	Order of ESO	ω_C	ω_O	b
Area 1	4	4	20	78.7739
Area 2	4	4	20	76.2598
Area 3	4	4	20	74.2768

Table 5: GALMI tuned PI controller parameters [23]

	Area 1	Area 2	Area 3
K_p	-3.27×10^{-4}	-6.96×10^{-4}	-1.60×10^{-4}
K_i	-0.3334	-0.3435	-0.3398

In case 1, the random load changes (P_{Li}), shown in Figure 18, are added to each area of the power systems. Figures 19, 20 and 21 show the ACE output, load frequency deviation Δf and the difference between control effort and load disturbance, which is ΔP_{err} ($\Delta P_{err} = \Delta P_C - \Delta P_L$) for both ADRC and PI controlled systems. From the simulations, we can see that both ADRC and the GALMI tuned PI controller can compensate the load fluctuations reflected by ΔP_{err} rapidly. However, the ACE, Δf, and ΔP_{err} of ADRC controller have less peak errors (the peak errors of the ACE and Δf for ADRC are no more than 0.05%) than the GALMI tuned PI controller. ADRC controlled system shows better transient responses than the PI controlled system.
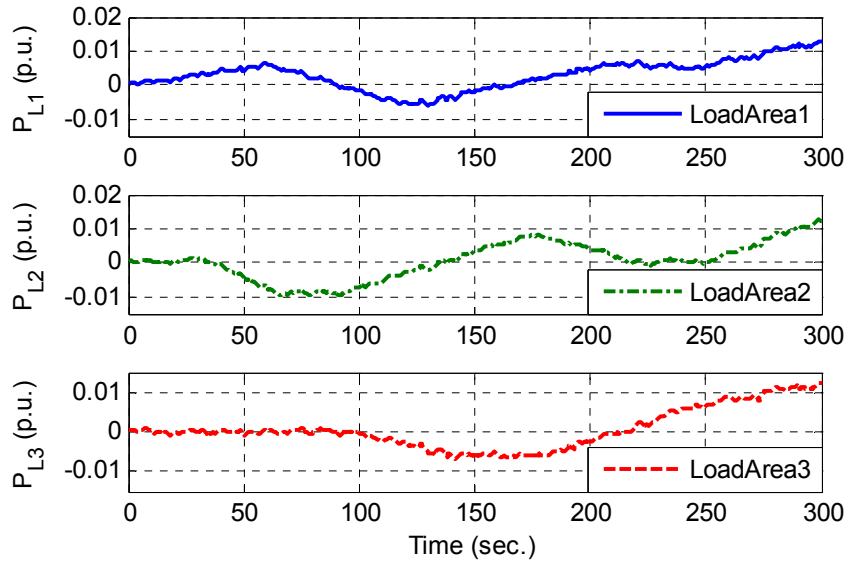
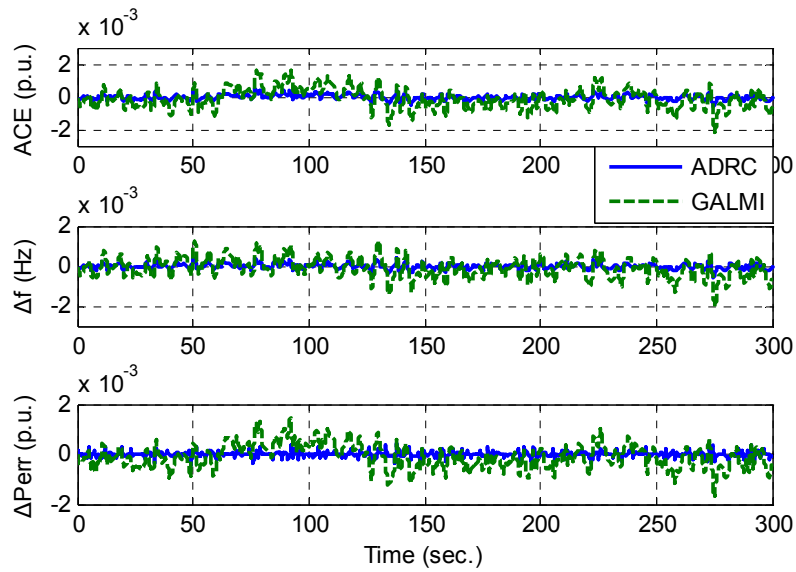*Figure 18: Random load changes*

Figure 19: System responses of area 1 for case 1
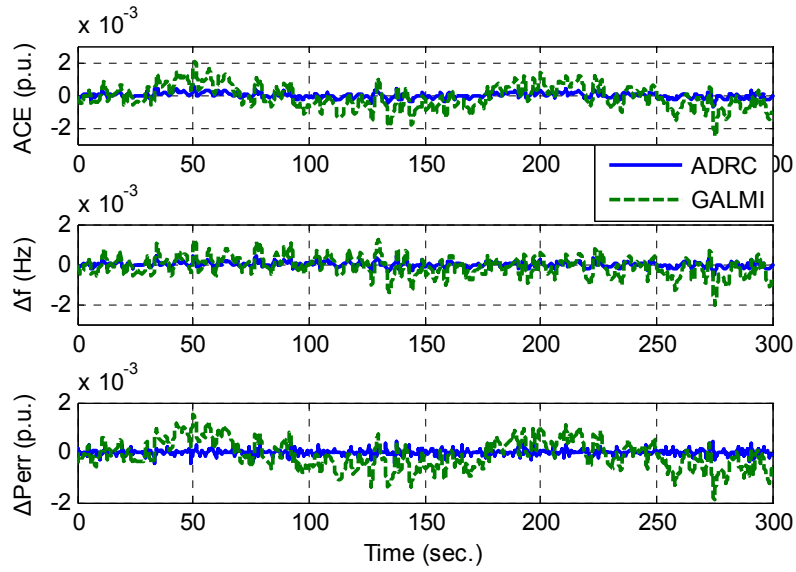
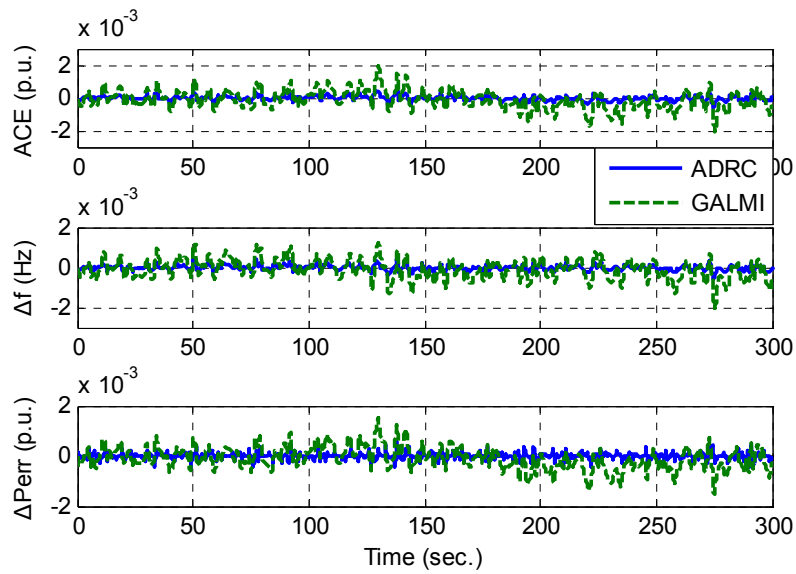*Figure 20: System responses of area 2 for case 1*

Figure 21: System responses of area 3 for case 1

In case 2, a step load change with large amplitude is added to each area. The purpose of this case is to test the robustness of the controllers against large disturbances. The

amplitudes of the load changes for the three areas are $\Delta P_{L1} = 100$ *MW (0.1 p.u.)*, $\Delta P_{L2} = 80$ *MW (0.08 p.u.)* and $\Delta P_{L3} = 50$ *MW (0.05 p.u.)* respectively. The power loads are added to the systems at $t = 2$ second. The ACE, Δf and the control effort for both ADRC and PI controlled systems are shown in Figures 22, 23 and 24. ADRC demonstrates smaller oscillations and faster responses in the ACE and Δf responses than that of the GALMI tuned PI controller. However, the control effort of ADRC shows an overshoot at the switching edge of the load change. This is due to a slight lag of ESO in response to the external disturbance. Nevertheless the overshoot magnitude of ADRC is reasonable. So it will not affect the implementation of the controller in practice.
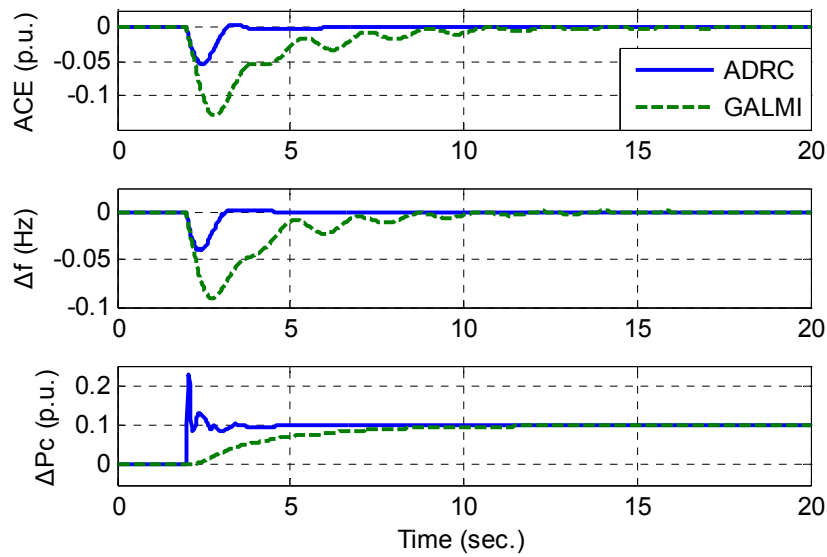

Figure 22: System responses of area 1 for case 2
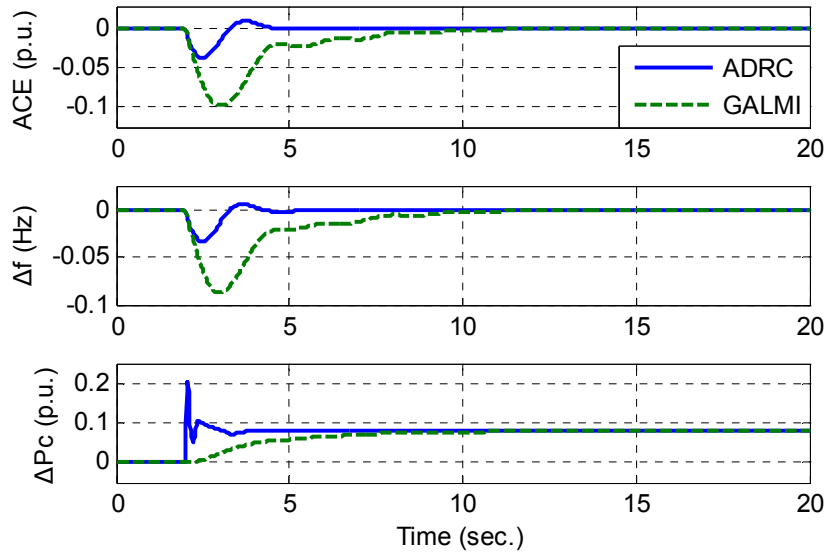
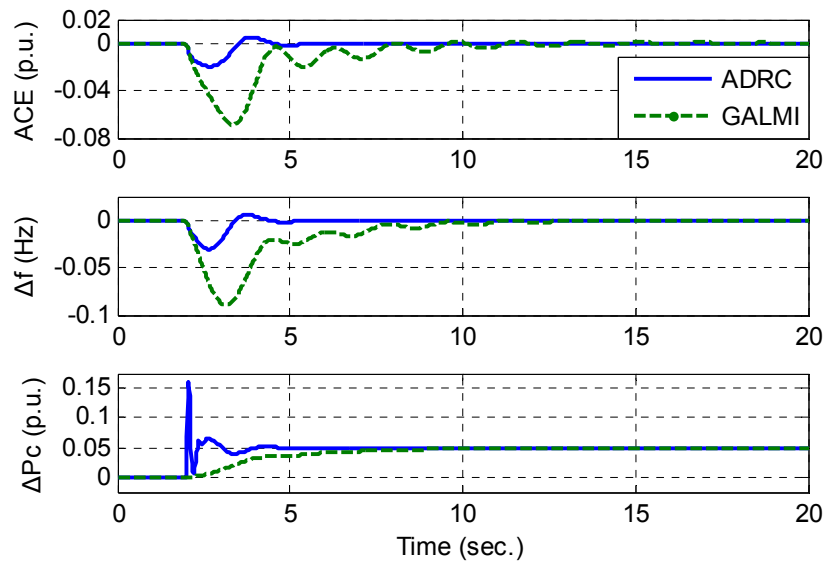*Figure 23: System responses of area 2 for case 2*

Figure 24: System responses of area 3 for case 2

In case 3, a common incident that could happen to real power systems is that one or several generating units go down. This kind of contingency requires the controllers to make

quick and correct adjustments to the whole power system. Otherwise the system might lose stability. Subsequently there would be power cut in a wide area. But if the load frequency controller can perform an effective response to such contingency, the whole system will face less risk of losing stability. So the purpose of case 3 is to test the stability and effectiveness of ADRC power system under an extreme condition that one generating unit fails to operate.

In order to simulate the extreme condition, the three-area non-reheat model is modified so that one generating unit is cut off from the whole system at a set time. For case 3, the same load changes as the ones in case 2 are added to the three areas at $t = 2$ second. Generating company 3 (GenCo3) is cut off at the 20th second while at the 30th second, another 100 MW (0.1 $p.u.$) step change is loaded on area 1. The responses of area 1 are shown in Figure 25. From the simulation result, we can see that after cutting off the generating company 3 (GenCo3), the GALMI based PI controller drives the ACE to zero with an obvious oscillation since the system model has changed significantly while ADRC is still able to effectively control the system output to track the reference with little overshoot and negligible oscillation. However, we should also notice that the control effort ΔP_C of the GALMI based PI controller is much smoother than ADRC. If the GALMI is tuned more aggressively, the level of the oscillation in ACE and Δf of the PI controller will be closer to the responses of ADRC, while the ΔP_C of the PI controller would look more similar to that of ADRC, too.
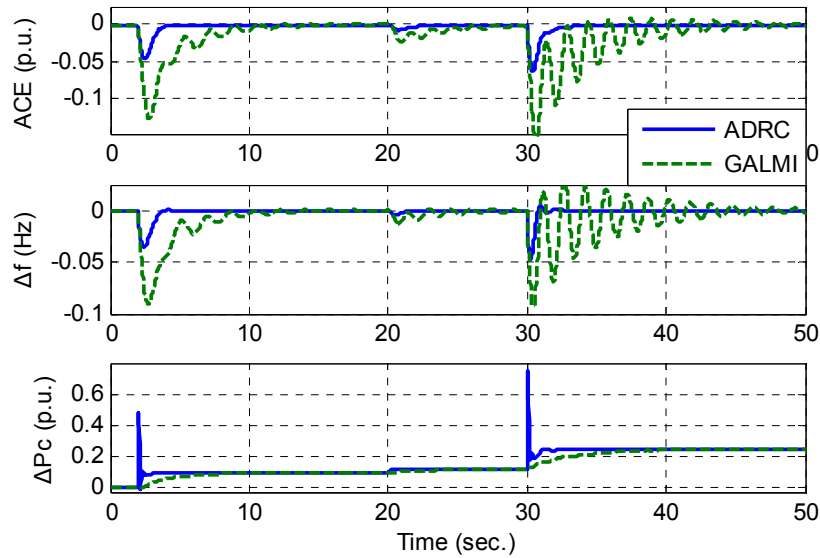
Figure 25: System responses of area 1 for case 3

GenCo 3 fails to operate at t = 20 sec.

Another 0.1 p.u. load disturbance was added to area one at t = 30 sec.

4.3 Summary of the chapter

The simulation results in this chapter verified the effectiveness of ADRC on the LFC problem in three aspects. First of all, ADRC is able to cancel the ACE to satisfy the LFC requirements of maintaining the standard frequency and keeping the tie-line power exchange according to the schedule. Secondly, ADRC is effective to cancel both random and large step types of load disturbances. Thirdly, ADRC is able to resist the interferences to the controller design of both parameter and model uncertainties. Thus, ADRC is considered to be a suitable LFC solution.

CHAPTER V

STABILITY AND ROBUSTNESS ANALYSES

In Chapter IV, the effectiveness and robustness of ADRC controlled power system have been demonstrated by time-domain simulation results. In this chapter, a transfer function representation of ADRC controlled power system will be developed. The robustness and stability of the control system will be investigated through frequency-domain analyses.

5.1 Transfer function development of the controlled system

The transfer function representation of ADRC was initially reported in [28], and then applied to MEMS devices in [33, 37]. In this section, the Laplace transform of ADRC controlled power system will be developed. Then the frequency-domain analyses will be conducted on the basis of the transfer function (TF) representation.

In this section, area 1 in Figure 9 will be utilized to develop the transfer function representation. This area is mainly composed of a decentralized power plant consisting of non-reheat turbine unit, governor, and generator, and an ADRC. The transfer functions between multiple system inputs (*R(s)*, *ΔP_L(s)* and *ΔP_tie(s)*) and the ACE output *Y(s)* for a decentralized non-reheat power generating area were given in (23)–(25) in Chapter II.

First let us develop the TF from the reference signal *R(s)* to the ACE output *Y(s)* while the other two inputs (*ΔP_L(s)* and *ΔP_tie(s)*) are set to be zeros. After letting *ΔP_L(s)* = 0 and *ΔP_tie(s)* = 0, (22) becomes

$$Y(s) = G_P(s)U(s). \tag{66}$$

The ESO in (51) can be rewritten as

$$sZ(s) = (A - LC)Z(s) + BU(s) + LY(s). \tag{67}$$

The control law obtained from (54) and (56) can be represented by

$$U(s) = k_1 R(s)/b - KZ(s)/b, \tag{68}$$

where $K = \begin{bmatrix} k_1 & k_2 & k_3 & 1 \end{bmatrix}$. Substituting *U(s)* in (67) with (68) yields

$$Z(s) = [T(s)]^{-1} [Bk_1 R(s)/b + LY(s)], \tag{69}$$

where

$$T(s) = sI - A + LC + BK/b. \tag{70}$$

Replacing $Z(s)$ in (67) with (69) gives

$$U(s) = G_{PF}(s)G_{EC}(s)R(s) - G_{EC}(s)Y(s),$$
(71)

where $G_{EC}(s)$ is represented by

$$G_{EC}(s) = K\left[T(s)\right]^{-1} L/b$$
(72)

and $G_{PF}(s)$ is a pre-filter represented by

$$G_{PF}(s) = \left[k_1\left(b - K\left[T(s)\right]^{-1} B\right)\right]\Big/\left(bK\left[T(s)\right]^{-1} L\right).$$
(73)

Replacing the $U(s)$ in (66) with (71), we have

$$G_{cl}(s) = \frac{Y(s)}{R(s)} = \frac{G_{PF}(s)G_{EC}(s)G_P(s)}{1 + G_{EC}(s)G_P(s)}.$$
(74)

Then let us develop the TF from the power load disturbance $\Delta P_L(s)$ to the ACE output $Y(s)$. Again, we need to set the other two inputs to zeros. With $\Delta P_{tie}(s) = 0$, (22) becomes

$$Y(s) = G_P(s)U(s) + G_D(s)\Delta P_L(s).$$
(75)

With $R(s) = 0$, (71) becomes

$$U(s) = -G_{EC}(s)Y(s).$$
(76)

Replacing $U(s)$ in (75) with (76), we obtain the transfer function $G_{Dcl}(s)$ from $\Delta P_L(s)$ to $Y(s)$ as

$$G_{Dcl}(s) = \frac{Y(s)}{\Delta P_L(s)} = \frac{G_D(s)}{1 + G_P(s)G_{EC}(s)} . \tag{77}$$

Similarly, when $\Delta P_L(s) = 0$ and $R(s) = 0$, we can get the transfer function $G_{tiecl}(s)$ from $\Delta P_{tie}(s)$ to $Y(s)$ as

$$G_{tiecl}(s) = \frac{Y(s)}{\Delta P_{tie}(s)} = \frac{G_{tie}(s)}{1 + G_P(s)G_{EC}(s)} . \tag{78}$$

According to (71)–(73), (77) and (78), the closed-loop control system for the one-area power system with non-reheat turbine unit will be constructed as Figure 26. From Figure 26, we can see that the open-loop transfer function is

$$G_O(s) = G_{EC}(s)G_P(s) . \tag{79}$$

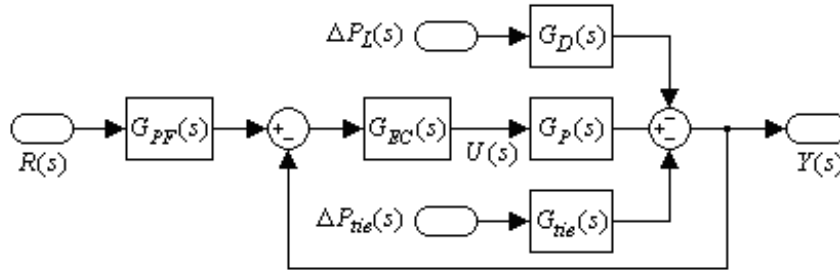Figure 26: Block diagram of the closed-loop control system

5.2 Stability and robustness against parameter uncertainties

The frequency responses of the open-loop transfer function (79) are shown in Figure 27, where the parameters of the non-reheat unit (M_1, D_1, T_{ch1}, T_{g1}, R_1, and T_1) in the first test power system are varying from −20% to 20% of their nominal values. The

corresponding gain and phase margins are shown in Table 6. The Bode diagram (Figure 27) shows that the designed ADRC is able to maintain the stability of the system against ±20% parameter variations of the selected unit. This result, together with the time-domain responses (Figures 13, 14 and 15), proved the stability and the strong robustness of the control system against parameter uncertainties.
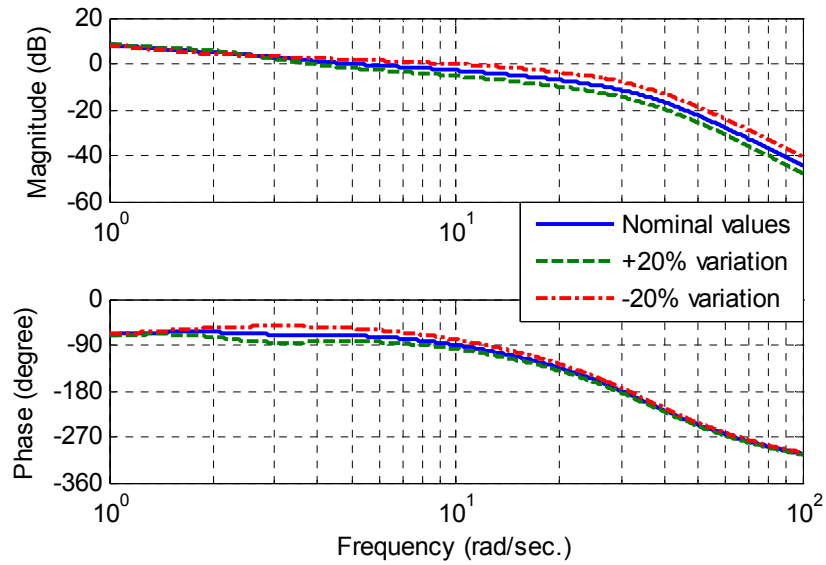

Figure 27: Frequency responses of $G_O(s)$ with different parameters for the non-reheat area

Table 6: Stability margins of the parameter varying test

Parameter values	Gain margin (dB)	Phase margin (deg.)
Nominal	11.5	108
+20%	14.0	96
−20%	8.5	103

5.3 External disturbance rejection

We have obtained the closed-loop transfer function from power load disturbance $\Delta P_L(s)$ to ACE output $Y(s)$ in (77). The Bode diagram of the transfer function is shown in Figure 28 for the non-reheat area with varying parameters (M_1, D_1, T_{ch1}, T_{g1}, R_1, and T_1) from −20% to 20% of their nominal values. The results in Figure 28 demonstrate the disturbance rejection ability of the designed controller since the magnitude responses are under 0 *dB* at any input frequency. The frequency responses are almost unchanged in this figure with the variations of the system parameters. The unchanged frequency responses also verified the robustness of the control system in the presences of both disturbance and parameter uncertainties.
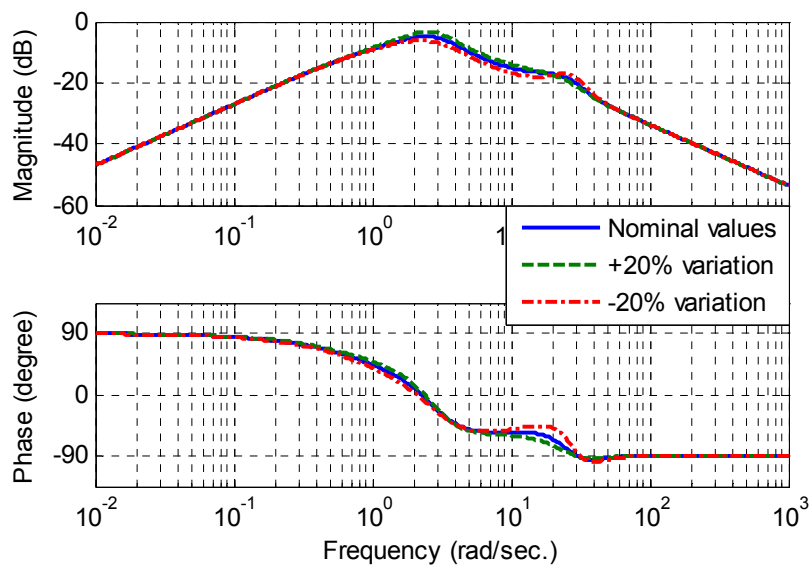
Figure 28: Frequency responses of $G_{Dcl}(s)$ with variant parameters for the non-reheat area

5.4 Stability and robustness against model uncertainties

In this section, we will utilize the second test power system introduced in Section IV.2 to test the stability and robustness of ADRC system. The structure of this test power system was shown in Figure 16. For contingency test, we suppose two extreme situations. In this first situation, the power generating company GenCo2 fails to operate. In the second extreme situation, both the power generating companies GenCo2 and GenCo3 fail to operate. In both situations, the controller parameters of ADRC remain unchanged. Then the Bode diagram of the open-loop transfer function (79) with the unchanged ADRC is shown in Figure 29. The stability margins of the Bode diagram are listed in Table 7. From the Bode diagram and the stability margins, we can see that ADRC is quite stable and reliable under the extreme situations.
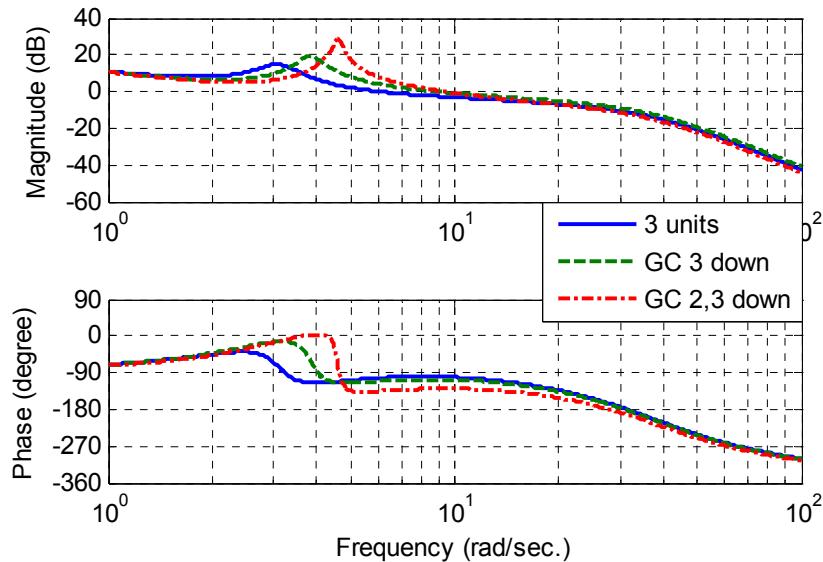
Figure 29: Bode diagram of the open-loop transfer function $G_O(s)$ with model uncertainties

Table 7: Stability margins of the model varying test

GenCos situation	Gain margin (dB)	Phase margin (deg.)
Normal	11.2	77
GenCo 3 fails to operate	9.4	74
GenCo 2 & 3 fail to operate	10.7	51

5.5 Summary of the chapter

This chapter applied frequency-domain analyses to ADRC controlled power system. The Bode diagrams further demonstrated the notable robustness of ADRC against parameter and model uncertainties. They also demonstrate the reliability of the control system in extreme situations. The stability margins prove the stability of the control system.

CHAPTER VI

CONCLUSIONS AND FUTURE RESEARCH

6.1 Conclusions

This thesis proposed an ADRC based decentralized load frequency controller for interconnected power systems. The design approaches of ADRC have been explained in detail. Two types of power systems were established and utilized to test the stability, reliability and robustness of ADRC controlled system in the presences of power load changes, system parameter variations, and crashing of generating units. The two test systems are a three-area three-different-unit power system including reheat, non-reheat, and hydraulic units and a three-area nine-unit power system consisted of only non-reheat units. ADRC was simulated on the two types of test systems respectively. The simulation results in time-domain verified the effectiveness of ADRC through successfully regulating the ACE outputs, frequency errors and tie-line power errors in the presences of external disturbance, parameter

uncertainties and accidental crashing of generating units, which represents the structural or model uncertainties.

In addition, the transfer function representations of ADRC controlled power system were developed. Frequency-domain analyses were conducted on the basis of the transfer function representations. The Bode diagrams and stability margins obtained from the frequency-domain analyses further confirmed the stability, reliability, and robustness of ADRC. .

ADRC has been applied to multiple areas including MEMS, chemical industry, and aerospace etc. The thesis initiates the successful employment of ADRC technology for power systems.

6.2 Future work

In the future, the following research on both ADRC and the power system is expected to be conducted.

6.2.1 Improvement of ADRC

As an increasingly popular practical control method, ADRC has the advantage of requiring little information from the plant and notable robustness against parameter and

model uncertainties. But as a novel control technique, it could be improved in the following aspect.

In the thesis, the designed ADRC can guarantee the fast response of the ACE with small overshoot. However, during the process of simulating ADRC in a power system, the magnitude of the control effort shows a big peak value at the initial stage of the simulation. As we reduce the control effort at the initial stage with a limiter, the control performance will be degraded. In the future, we will need to find a balance between changing the control effort of ADRC and obtaining the optimal ACE response. Through tuning the bandwidths of the ESO and the state feedback controller, we could possibly regulate the relationship between the control effort and the response. But a quantitative method is needed to determine the controller parameters of ADRC. Those optimization algorithms such as GA and LMI could be applied to tune the parameters in ADRC.

6.2.2 Improvement of the ESO

In real power systems, the large step power load disturbances are discontinuous. The linear ESO used in the thesis has the limitation of requiring the disturbance to change smoothly instead of discontinuously. Thus the discontinuous disturbance can not be accurately estimated by the linear ESO no matter how we tune the bandwidths of the ESO and the state feedback controller. Therefore, in the future, non-linear parts will be included in the ESO or even the whole ADRC to obtain a more accurate approximation of the discontinuous load disturbance, and hence to make ADRC a more powerful control technique for the power system.

6.2.3 Improvement of the model and control of the power systems

For the LFC problem, some of the plant limits such as generation rate constraints and deadbands are disregarded in this thesis. However, in reality, they exist in power systems. In the future, we plan to include the plant limits in the model of the power system to make the model more practical. Accordingly, we will also modify ADRC so as to successfully apply it to the new model.

In this thesis, the general engineering tool MATLAB/Simulink is used to simulate ADRC in the power system. In the future, we plan to construct the power system in a special software package named Simplorer®, which is a very powerful CAD tool in modeling real systems with power electronics and electromechanics. Simplorer could provide more realistic power generating units just like the ones in the real world. The successful implementation of ADRC on such a Simplorer based power system model will ensure its feasibility in power industries.

REFERENCE

[1] P. Kundur, *Power System Stability and Control.* New York: McGraw-Hill, 1994.

[2] S. Ohba, H. Ohnishi, and S. Iwamoto, "An Advanced LFC Design Considering Parameter Uncertainties in Power Systems," *Proceedings of IEEE conference on Power Symposium,* pp. 630–635, Sep. 2007.

[3] A. Morinec, and F. Villaseca, "Continuous-Mode Automatic Generation Control of a Three-Area Power System," *The 33rd North American Control Symposium,* pp. 63–70, 2001.

[4] M. Kothari, N. Sinha and M. Rafi, "Automatic Generation Control of an Interconnected Power System under Deregulated Environment," *Power Quality,* vol. 18, pp. 95–102, Jun. 1998.

[5] V. Donde, M. A. Pai, and I. A. Hiskens, "Simulation and Optimization in an AGC System after Deregulation," *IEEE Transactions on Power Systems,* vol. 16, pp. 481–489, Aug. 2001.

[6] M. Aldeen, and R. Sharma, "Robust Detection of Faults in Frequency Control Loops," *IEEE Transactions on Power Systems,* vol. 22, no. 1, pp. 413–422, Feb. 2007.

[7] Y. Moon, H. Ryu, B. Choi, and H. Kook, "Improvement of System Damping by Using the Differential Feedback in the Load Frequency Control," *IEEE Power Engineering Society 1999 Winter Meeting,* vol. 1, pp. 683–688, Feb. 1999.

[8] Y. Moon, H. Ryu, J. Lee, and S. Kim, "Power System Load Frequency Control Using Noise-Tolerable PID Feedback," *IEEE International Symposium on Industrial Electronics,* vol. 3, pp. 1714–1718, Jun. 2001.

[9]   Y. Moon, H. Ryu, B. Choi, and B. Cho, "Modified PID Load-Frequency Control with the Consideration of Valve Position Limits," *IEEE Power Engineering Society 1999 Winter Meeting,* vol. 1, pp. 701–706, Feb. 1999.

[10] D. Rerkpreedapong, and A. Feliachi, "PI Gain Scheduler for Load Frequency Control Using Spline Techniques," *The 35th Southeastern Symposium on System Theory,* pp. 259–263, Mar. 2003.

[11] M. Rahi, and A. Feliachi, "H_∞ Robust Decentralized Controller for Nonlinear Power Systems," *The 30th Southeastern Symposium of System Theory*, pp. 268–270, Mar. 1998.

[12] I. Ngamroo, Y. Mitani, and K. Tsuji, "Robust Load Frequency Control by Solid-State Phase Shifter Based on H_∞ Control Design," *IEEE Power Engineering Society 1999 Winter Meeting,* vol. 1, pp. 725–730, Feb. 1999.

[13] A. Bensenouci, and A. Ghany, "Mixed H_∞/H_2 with Pole-Placement Design of Robust LMI-Based Output Feedback Controllers for Multi-Area Load Frequency Control," *Proceedings of The International Conference on Computer as a Tool,* pp. 1561–1566, Sep. 2007.

[14] D. Rerkpreedapong, and A. Feliachi, "Decentralized H_∞ Load Frequency Control Using LMI Control Toolbox," *The 2003 International Symposium on Circuits and Systems,* vol. 3, no. 25–28, pp. 411–414, May 2003.

[15] A. Paradkar, A. Davari, and A. Feliachi, "Disturbance Accommodation Control versus Conventional Control, in LFC of a Two Area Distribution System in a Deregulated Environment," *The 35th Southeastern Symposium on System Theory,* pp. 98–102, Mar. 2003.

[16] Y. Moon, H. Ryu, B. Kim, and K. Song, "Optimal Tracking Approach to Load Frequency Control in Power Systems," *IEEE Power Engineering Society 2000 Winter Meeting,* vol. 2, pp. 1371–1376, Jan. 2000.

[17] L. Kong, and L. Xiao, "A New Model Predictive Control Scheme-Based Load-Frequency Control," *Proceedings of IEEE International Conference on Control and Automation,* pp. 2514–2518, Jun. 2007.

[18] B. Bakken, and O. Grande, "Automatic Generation Control in a Deregulated Power System," *IEEE Transactions on Power Systems,* vol. 13, no. 4, pp. 1401–1406, Nov. 1998.

[19] Ibraheem, P. Kumar, and D. Kothari, "Recent Philosophies of Automatic Generation Control Strategies in Power Systems," *IEEE Transactions on Power Systems,* vol. 20, no. 1, pp. 346–357, Feb. 2005.

[20] T. Hiyama, S. Koga, and Y. Yoshimuta, "Fuzzy Logic Based Multi-Functional Load Frequency Control," *IEEE Power Engineering Society 2000 Winter Meeting,* vol. 2, pp. 921–926, Jan. 2000.

[21] K. Yukita, Y. Goto, K. Mizuno, T. Miyafuji, K. Ichiyanagi, and Y. Mizutani, "Study of Load Frequency Control using Fuzzy Theory by Combined Cycle Power Plant," *IEEE Power Engineering Society 2000 Winter Meeting,* vol. 1, pp. 422–427, Jan. 2000.

[22] H. Mohamed, L. Hassan, M. Moghavvemi, and S. Yang, "Load Frequency Controller Design for Iraqi National Super Grid System Using Fuzzy Logic Controller," *SICE Annual Conference,* pp. 227–232, Aug. 2008.

[23] D. Rerkpreedapong, A. Hasanovic, and A. Feliachi, "Robust Load Frequency Control Using Genetic Algorithms and Linear Matrix Inequalities," *IEEE Transactions on Power Systems*, vol. 18, no. 2, pp. 855–861, May 2003.

[24] Z. Gao, Y. Huang, and J. Han, "An Alternative Paradigm for Control System Design," *Proceedings of IEEE Conference on Decision and Control,* vol. 5, no. 4–7, pp. 4578–4585, Dec. 2001.

[25] Z. Gao, "Active Disturbance Rejection Control: A Paradigm Shift in Feedback Control System Design," *Proceedings of American Control Conference*, pp. 2399–2405, Jun. 2006.

[26] Z. Gao, "Scaling and Parameterization Based Controller Tuning," *Proceedings of American Control Conference,* vol. 6, no. 4–6, pp. 4989–4996, June 2003.

[27] R. Miklosovic, and Z. Gao, "A Robust Two-Degree-of-Freedom Control Design Technique and Its Practical Application," *The 39th IAS Annual Meeting, Industry Applications Conference,* vol. 3, pp. 1495–1502, Oct. 2004.

[28] G. Tian, and Z. Gao, "Frequency Response Analysis of Active Disturbance Rejection Based Control System," *Proceedings of IEEE International Conference on Control Applications,* pp. 1595–1599, Oct. 2007.

[29] B. Sun, and Z. Gao, "A DSP-Based Active Disturbance Rejection Control Design for a 1-kW H-bridge DC-DC Power Converter," *IEEE Transactions on Industrial Electronics,* vol. 52, no.5, pp. 1271–1277, Oct. 2005.

[30] Z. Chen, Q. Zheng, and Z. Gao, "Active Disturbance Rejection Control of Chemical Processes," *Proceedings of IEEE International Conference on Control Applications,* pp. 855–861, Oct. 2007.

[31] W. Zhou, and Z. Gao, "An Active Disturbance Rejection Approach to Tension and Velocity Regulations in Web Processing Lines," *IEEE International Conference on Control Applications,* pp. 842–848, Oct. 2007.

[32] L. Dong, Q. Zheng, and Z. Gao, "A Novel Oscillation Controller for Vibrational MEMS Gyroscopes," *Proceedings of American Control Conference,* pp. 3204–3209, Jul. 2007.

[33] L. Dong, and D. Avanesian, "Drive-mode Control for Vibrational MEMS Gyroscopes," *IEEE Transactions on Industrial Electronics*, vol. 56, no. 4, pp. 956–963, 2009.

[34] L. Dong, Q. Zheng, and Z. Gao, "On Control System Design for the Conventional Mode of Operation of Vibrational Gyroscopes," *IEEE Sensors Journal*, vol. 8, no. 11, pp. 1871–1878, Nov. 2008.

[35] Q. Zheng, L. Dong, D. Lee, and Z. Gao, "Active Disturbance Rejection Control and Implementation for MEMS Gyroscopes," to appear in *IEEE Transactions on Control System Technology*, 2009.

[36] Y. Zhang, L. Dong, and Z. Gao, "Load Frequency Control for Multiple-Area Power Systems", to appear in *Proceedings of American Control Conference*, St. Louis, Mo, Jul. 2009.

[37] J. Edwards, "Modeling and Feedback Control of a MEMS Electrostatic Actuator", *Master's Thesis,* Department of Electrical and Computer Engineering, Cleveland State University, May 2009.